caspase-independent cell death, possibly due to enzymatic over-activation [33-35]. We also observed that co-treatment of Bcl-xL-overexpressing Ms-1 cells with incednine and ant-tumor drugs induced AIF release and subsequent caspase-independent cell death (unpublished data); therefore, we can not exclude the possibility that incednine binds to PARP1 and functions as PARP1 agonist by accerelating AIF release.

However, the most likely candidate of an incednine target protein is ACACA (acetyl-CoA carboxylase-α), which was classified in cluster 9. ACACA is the rate-limiting enzyme for long-chain fatty acid synthesis that catalyzes the ATP-dependent carboxylation of acetyl-CoA to malonyl-CoA, playing a critical role in cellular energy storage and lipid synthesis [36]. There is strong evidence that cancer cell proliferation and survival are dependent on *de novo* fatty acid synthesis [37-40]. Additionally, ACACA is upregulated in multiple types of human cancers [41,42]; therefore, ACACA may also contribute to cell survival in Bcl-xL-overexpressing tumor cells. Indeed, our preliminary experiments suggested that chemical inhibition of ACACA using TOFA (5-tetradecyloxy-2-furoic acid, ACACA antagonist) or small interfering RNA-mediated ACACA silencing results in the induction of apoptosis in Bcl-xL-overexpressing human small cell lung carcinoma Ms-1 cells when combined with anti-tumor drugs as does incednine (unpublished observation), suggesting that ACACA might be a molecular target of incednine. The possibility that incednine targets ACACA is being actively investigated.

While our experimental verification implied the relatively low precision value 28.6% (2/7), new detections of two incednine-binding proteins in addition to previously identified 53 proteins are significant. On the other hand, while we selected 7 candidates by clustering 182 predicted proteins for experimental verification, more comprehensive verification experiments for the 182 predicted proteins are needed.

The application of our method to incednine resulted in 28.6% (2/7) precision according to *in vitro* pull-down assay. However, this relatively low precision value does not represent the true statistical significance of the method and is not comparable to the benchmark performances (including 98.4% precision) by 10-fold cross-validation for COPICAT system.

This 28.6% precision can be evaluated by using the following *P*-value.

$$P\text{-}value = \sum_{x=p}^{t} \frac{{}_{M}C_{x} \times {}_{(N-M)}C_{(t-x)}}{{}_{N}C_{t}}$$

Here, N is the number of human proteins, M is the number of proteins potentially binding to the incednine, t is the number of tested proteins, and p is the number of true positives. With N =24,245, which is the number of human proteins in the KEGG repository, and $M = N \times 1\% \fallingdotseq 243$, which is based on the overestimated assumption that 1% of all proteins could be regarded as potential binding proteins for the incednine. This *P*-value defines the probability that the prediction precision can be obtained by random selection of proteins. Then, *P*-value of 0.002 was obtained for the prediction precision 28.6%. This small *P*-value means that 28.6% (2/7) precision can be obtained with very small chance by random selection, and therefore, this small *P*-value proves the validity of our method.

Conclusions

Although further study is required for complete determination of the target protein of incednine, this study demonstrated that our proposed protocol of predicting target protein combining *in silico* screening and experimental verification is useful, and provides new insight into a strategy for identifying target proteins of small molecules.

Methods

Training datasets

The DrugBank dataset was constructed from Approved DrugCards data, which were downloaded from the DrugBank database [20]. These data consist of 964 approved drugs and their 456 associated target proteins, constituting 1,731 interacting pairs or positives. Additional data about 53 interactions with incednine, listed in Table 1, were obtained from our previous binding experiments.

Feature vectors

An amino acid sequence of protein is divided into trimers (three amino acid residues), and all of the 8,000 trimers are clustered into 199 groups according to physical-chemical properties. Then, an amino acid sequence is converted to a 199-dimensional feature vector based on the frequencies of 199 clusters (See for [13] the details of this procedure). A chemical compound is also converted to another feature vector of 199 dimension representing substructure statistics extracted from the structural formula of a chemical compound. The size of the dimensions, that is, 199 dimensions, was determined based on the variance of each dimension. The top 199 dimensions with significantly diverse variances in statistical classification were selected.

Statistical prediction method for protein-chemical interaction

We developed a comprehensively applicable statistical prediction method for interactions between any proteins

and chemical compounds, which requires only protein sequence data and chemical structure data and utilizes the statistical learning method of Support Vector Machines (SVM)[13,14].

We consider the problem as the binary classification of protein-chemical pairs whose abstractive identities are represented numerically by the 199 dimensional feature vectors defined above. We obtained a "positive" sample set, i.e., a set of protein-chemical pairs that have been proven to interact with each other via biological assays, from the DrugBank database [20]. Along with the positive sample set, SVM-based classifiers require a "negative" sample set, i.e., a set of protein-chemical pairs that do not interact with each other. Such a negative sample set can be extracted randomly from the whole complement set of the positive sample set. Though we used random pairs of drugs and proteins as negative samples in constructing a model, the lack of reliable negative samples is always a problem when applying the statistical learning methods. In our current study, it is assumed that drugs in the DrugBank dataset rarely interact with proteins other than their known targets because they are approved drugs. Using the resultant positive and negative protein-chemical pair sets, we trained two-layer SVMs. First, we trained each multiple first-layer SVM with small sample sets designed with different criteria. Next, using another larger sample set, we trained a second-layer SVM whose input is a set of probabilities output from the firstlayer SVMs. The prediction performances were evaluated by 10-fold cross-validation using the DrugBank dataset. The sensitivity, specificity, precision, and accuracy were 0.954, 0.999, 0.984, and 0.997, respectively, in cross-validation. The details of the algorithms and their prediction accuracy are described in our previous reports [13,14].

Support vector machines

Given n samples, each of which has an m-dimensional feature vector $\left(x_i = \left(x_i^1, \ldots, x_i^m\right)\right)$ and one of two classes, such as binding and non-binding $(y \in \{1, -1\})$, an SVM produces the classifier

$$f(x) = sign\left(\sum_{i=1}^{n} \alpha_i y_i K(x_i, x) + b\right),$$

where x is any new object which needs to be classified, $K(\cdot,\cdot)$ is a kernel function which indicates that the similarity between two vectors and $(\alpha_1, \cdots, \alpha_n)$ are the learned parameters. The RBF kernel $K(S_1, S_2) = \exp(-\gamma \| S_1 - S_2 \|)$ was utilized for the SVM classifier. In our study, the LIBSVM program [43] was employed to construct the SVM model.

Cell culture

Bcl-xL-overexpressing human SCLC Ms-1 cells [15] were maintained in Rosewell Park Memorial Institute media (Nissui, Japan) supplemented with 5% fetal bovine serum, 100 U/ml penicillin G, and 0.1 mg/mL kanamycin at 37°C in a humidified 5% CO_2 atmosphere.

Antibodies

Mouse monoclonal anti-DAPK1 (DAPK-55), rabbit monoclonal anti-PIK3CG (Y388), rabbit monoclonal anti-ACACA (EP687Y), mouse monoclonal anti-PIK3C2B, rabbit polyclonal anti-ITPR1, mouse monoclonal anti-PIP5K3, mouse monoclonal anti-CHD4, mouse polyclonal anti-GTF2IRD2, mouse polyclonal anti-PLCB1 antibodies were purchased from Abcam (Cambridge, MA). Rabbit polyclonal anti-KIF21B and mouse monoclonal anti-KIF5B (clone H2) antibodies were purchased from Millipore (Bedford, MA). Goat polyclonal anti-PARP14 and goat polyclonal anti-KIF1A were purchased from Santa Cruz Biotechnology (Santa Cruz, CA). Mouse monoclonal anti-Beclin (clone 20) antibody was purchased from BD Transduction Laboratories (San Diego, CA). Rabbit polyclonal anti-PARP1 antibody was purchased from Cell Signaling Technology (Beverly, MA). Rabbit polyclonal anti-RGPD5 antibody was purchased from Lifespan Biosciences (Seattle, WA). Mouse monoclonal anti-Flag (M2) antibody was purchased form Sigma (St. Louis, MO).

Horseradish peroxidase-conjugated anti-mouse IgG and anti-rabbit IgG secondary antibodies were purchased from GE Healthcare (Little Chalfont, UK). Horseradish peroxidase-conjugated anti-goat IgG was purchased from Santa Cruz Biotechnology.

Western blotting

Cell lysates were separated by SDS-PAGE and transferred to a PVDF membrane (Millipore) by electroblotting. After the membranes had been incubated with primary and secondary antibodies, the immune complexes were detected with an Immobilon Western kit (Millipore), and luminescence was detected with a LAS-1000 mini (Fujifilm, Tokyo, Japan).

Preparation of incednine and biotinylated incednine

Incednine was isolated from the culture broth of *Streptomyces* sp. ML694-90F3 [15]. To obtain biotinylated incednine (see Additional file 3), incednine (137.0 mg) and the amine-reactive biotin-X (100.0 mg; Invitrogen) were dissolved in 13.0 mL $CHCl_3$:MeOH (10:1). After stirring at 40°C for 20 h, the reaction mixture was concentrated to dryness. The residue was resolved in 50 mL $CHCl_3$:MeOH:H_2O (5:6:4) and partitioned three times under basic conditions. The lower layer of $CHCl_3$:MeOH:H_2O (5:6:4) was evaporated *in vacuo* to yield a brown residue. The residue was purified by HPLC

(Senshu Pak Pegasil ODS 30 x 250 mm) and eluted with MeOH:40 mM KH_2PO_4 aq. (70:30) to give 19.4 mg biotinylated incednine.

In vitro biotinylated incednine pull-down assay

Bcl-xL-overexpressiong Ms-1 cells were collected and sonicated twice in IP buffer (50 mM HEPES (pH 7.5), 150 mM NaCl, 2.5 mM EGTA, 1 mM EDTA, 1 mM DTT, and a protease inhibitor cocktail (Roche, Mannheim, Germany)) for 10 s. The cell lysates were centrifuged at 10,000*g* for 15 min at 4°C. The resulting supernatants were incubated with biotin (50 nmol) or biotinylated incednine (50 nmol) and avidin beads at 4°C for 3 h. The beads were washed three times with phosphate-buffered saline (PBS). The bound proteins were eluted with 2 mM biotin in PBS, and concentrated by a centrifugal filter device (Ultracel (YM-10); Millipore). The resulting proteins were boiled in SDS sample buffer for 5 min and subjected to western blotting.

Liquid chromatography-tandem mass spectrometry

Incednine binding proteins purified using biotinylated incednine / avidin beads, and flag-tagged incednine (see Additional file 4) / anti-Flag antibody were anaylzed by liquid chromatography-tandem mass spectrometry (LC–MS/MS) system as previously described, respectively [44,45].

Additional files

Additional file 1: Validation work for eIF4A3, PDI, PP2A and Hsp70.

Additional file 2: Proteins computationally predicted to bind to incednine (grouped into 11 clusters).

Additional file 3: A stucture of biotinylated incednine.

Additional file 4: Preparation of Flag-tagged Incednine [46,47].

Authors' contributions

YS and MI designed the study and analyzed the data. HK, HH, MN and YF performed the experiments. YS, MI and HK wrote the paper. YF synthesized biotinylated incednine. AI, MY, SI, KS, TD, TT, and TN performed MS/MS analysis. All authors read and approved the final manuscript.

Acknowledgements

This work was supported in part by a Grant program for bioinformatics research and development from the Japan Science and Technology Agency. This work was also supported by Grant-in-Aid for Scientific Research (A) No.23241066 from the Ministry of Education, Culture, Sports, Science and Technology of Japan.

Author details

[1]Department of Biosciences and Informatics, Faculty of Science and Technology, Keio University, 3-14-1 Hiyoshi, Kohoku-ku, Yokohama 223-8522, Japan. [2]Chemical Genetics Laboratory, RIKEN Advanced Science Institute, 2-1 Hirosawa, Wako-shi, Saitama 351-0198, Japan. [3]National Institute of Advanced Industrial Science and Technology (AIST), 2-4-7 Aomi, Koto-ku, Tokyo 135-0064, Japan. [4]Graduate School of Pharmaceutical Sciences, Tohoku University, 6-3 Aza-Aoba, Aramaki, Aoba, Sendai 980-8578, Japan. [5]Department of Applied Chemistry, Tokyo Institute of Technology, 2-12-1 Ookayama, Meguro, Tokyo 152-8552, Japan.

Received: 15 November 2011 Accepted: 5 April 2012
Published: 5 April 2012

References

1. Alaimo PJ, Shogren-Knaak MA, Shokat KM: **Chemical genetic approaches for the elucidation of signaling pathways.** *Curr Opin Chem Biol* 2001, **5**:360–367.
2. Zheng XF, Chan TF: **Chemical genomics in the global study of protein functions.** *Drug Discov Today* 2002, **7**:197–205.
3. Harding MW, Galat A, Uehling DE, Schreiber SL: **A receptor for the immunosuppressant FK506 is a cis-trans peptidyl-prolyl isomerase.** *Nature* 1989, **341**:758–760.
4. Liu J, Farmer JD Jr, Lane WS, Friedman J, Weissman I, Schreiber SL: **Calcineurin is a common target of cyclophilin-cyclosporin A and FKBP-FK506 complexes.** *Cell* 1991, **66**:807–815.
5. Flanagan WM, Corthesy B, Bram RJ, Crabtree GR: **Nuclear association of a T-cell transcription factor blocked by FK-506 and cyclosporin A.** *Nature* 1991, **352**:803–807.
6. Nishi K, Yoshida M, Fujiwara D, Nishikawa M, Horinouchi S, Beppu T: **Leptomycin B targets a regulatory cascade of crm1, a fission yeast nuclear protein, involved in control of higher order chromosome structure and gene expression.** *J Biol Chem* 1994, **269**:6320–6324.
7. Kudo N, Matsumori N, Taoka H, Fujiwara D, Schreiner EP, Wolff B, Yoshida M, Horinouchi S: **Leptomycin B inactivates CRM1/exportin 1 by covalent modification at a cysteine residue in the central conserved region.** *Proc Natl Acad Sci U S A* 1999, **96**:9112–9117.
8. Yoshida M, Kijima M, Akita M, Beppu T: **Potent and specific inhibition of mammalian histone deacetylase both in vivo and in vitro by trichostatin A.** *J Biol Chem* 1990, **265**:17174–17179.
9. Whitesell L, Mimnaugh EG, De Costa B, Myers CE, Neckers LM: **Inhibition of heat shock protein HSP90-pp 60v-src heteroprotein complex formation by benzoquinone ansamycins: essential role for stress proteins in oncogenic transformation.** *Proc Natl Acad Sci U S A* 1994, **91**:8324–8328.
10. Stebbins CE, Russo AA, Schneider C, Rosen N, Hartl FU, Pavletich NP: **Crystal structure of an Hsp90-geldanamycin complex: targeting of a protein chaperone by an antitumor agent.** *Cell* 1997, **89**:239–250.
11. Prodromou C, Roe SM, O'Brien R, Ladbury JE, Piper PW, Pearl LH: **Identification and structural characterization of the ATP/ADP-binding site in the Hsp90 molecular chaperone.** *Cell* 1997, **90**:65–75.
12. Hart CP: **Finding the target after screening the phenotype.** *Drug Discov Today* 2005, **10**:513–519.
13. Nagamine N, Sakakibara Y: **Statistical prediction of protein chemical interactions based on chemical structure and mass spectrometry data.** *Bioinformatics* 2007, **23**:2004–2012.
14. Nagamine N, Shirakawa T, Minato Y, Torii K, Kobayashi H, Imoto M, Sakakibara Y: **Integrating statistical predictions and experimental verifications for enhancing protein-chemical interaction predictions in virtual screening.** *PLoS Comput Biol* 2009, **5**:e1000397.
15. Futamura Y, Sawa R, Umezawa Y, Igarashi M, Nakamura H, Hasegawa K, Yamasaki M, Tashiro E, Takahashi Y, Akamatsu Y, *et al*: **Discovery of incednine as a potent modulator of the anti-apoptotic function of Bcl-xL from microbial origin.** *J Am Chem Soc* 2008, **130**:1822–1823.
16. Michelle L, Cloutier A, Toutant J, Shkreta L, Thibault P, Durand M, Garneau D, Gendron D, Lapointe E, Couture S, *et al*: **Proteins Associated with the Exon Junction Complex Also Control the Alternative Splicing of Apoptotic Regulators.** *Mol Cell Biol* 2012, **32**:954–967.
17. Lovat PE, Corazzari M, Armstrong JL, Martin S, Pagliarini V, Hill D, Brown AM, Piacentini M, Birch-Machin MA, Redfern CP: **Increasing melanoma cell death using inhibitors of protein disulfide isomerases to abrogate survival responses to endoplasmic reticulum stress.** *Cancer Res* 2008, **68**:5363–5369.
18. Didelot C, Lanneau D, Brunet M, Joly AL, De Thonel A, Chiosis G, Garrido C: **Anti-cancer therapeutic approaches based on intracellular and extracellular heat shock proteins.** *Curr Med Chem* 2007, **14**:2839–2847.
19. Lu J, Kovach JS, Johnson F, Chiang J, Hodes R, Lonser R, Zhuang Z: **Inhibition of serine/threonine phosphatase PP2A enhances cancer chemotherapy by blocking DNA damage induced defense mechanisms.** *Proc Natl Acad Sci U S A* 2009, **106**:11697–11702.
20. Wishart DS, Knox C, Guo AC, Shrivastava S, Hassanali M, Stothard P, Chang Z, Woolsey J: **DrugBank: a comprehensive resource for in silico drug discovery and exploration.** *Nucleic Acids Res* 2006, **34**:D668–D672. Database issue.

21. Stephens LR, Eguinoa A, Erdjument-Bromage H, Lui M, Cooke F, Coadwell J, Smrcka AS, Thelen M, Cadwallader K, Tempst P, *et al*: **The G beta gamma sensitivity of a PI3K is dependent upon a tightly associated adaptor, p101.** *Cell* 1997, **89**:105–114.
22. Engelman JA, Luo J, Cantley LC: **The evolution of phosphatidylinositol 3-kinases as regulators of growth and metabolism.** *Nat Rev Genet* 2006, **7**:606–619.
23. Hickey FB, Cotter TG: **BCR-ABL regulates phosphatidylinositol 3-kinase-p110gamma transcription and activation and is required for proliferation and drug resistance.** *J Biol Chem* 2006, **281**:2441–2450.
24. Edling CE, Selvaggi F, Buus R, Maffucci T, Di Sebastiano P, Friess H, Innocenti P, Kocher HM, Falasca M: **Key role of phosphoinositide 3-kinase class IB in pancreatic cancer.** *Clin Cancer Res* 2010, **16**:4928–4937.
25. Ame JC, Spenlehauer C, de Murcia G: **The PARP superfamily.** *Bioessays* 2004, **26**:882–893.
26. Kim MY, Zhang T, Kraus WL: **Poly(ADP-ribosyl)ation by PARP-1: 'PAR-laying' NAD+ into a nuclear signal.** *Genes Dev* 2005, **19**:1951–1967.
27. Herceg Z, Wang ZQ: **Functions of poly(ADP-ribose) polymerase (PARP) in DNA repair, genomic integrity and cell death.** *Mutat Res* 2001, **477**:97–110.
28. Wang ZQ, Stingl L, Morrison C, Jantsch M, Los M, Schulze-Osthoff K, Wagner EF: **PARP is important for genomic stability but dispensable in apoptosis.** *Genes Dev* 1997, **11**:2347–2358.
29. Helleday T, Petermann E, Lundin C, Hodgson B, Sharma RA: **DNA repair pathways as targets for cancer therapy.** *Nat Rev Cancer* 2008, **8**:193–204.
30. Farmer H, McCabe N, Lord CJ, Tutt AN, Johnson DA, Richardson TB, Santarosa M, Dillon KJ, Hickson I, Knights C, *et al*: **Targeting the DNA repair defect in BRCA mutant cells as a therapeutic strategy.** *Nature* 2005, **434**:917–921.
31. Albert JM, Cao C, Kim KW, Willey CD, Geng L, Xiao D, Wang H, Sandler A, Johnson DH, Colevas AD, *et al*: **Inhibition of poly(ADP-ribose) polymerase enhances cell death and improves tumor growth delay in irradiated lung cancer models.** *Clin Cancer Res* 2007, **13**:3033–3042.
32. Veuger SJ, Curtin NJ, Richardson CJ, Smith GC, Durkacz BW: **Radiosensitization and DNA repair inhibition by the combined use of novel inhibitors of DNA-dependent protein kinase and poly(ADP-ribose) polymerase-1.** *Cancer Res* 2003, **63**:6008–6015.
33. Yu SW, Wang H, Poitras MF, Coombs C, Bowers WJ, Federoff HJ, Poirier GG, Dawson TM, Dawson VL: **Mediation of poly(ADP-ribose) polymerase-1-dependent cell death by apoptosis-inducing factor.** *Science* 2002, **297**:259–263.
34. Cregan SP, Dawson VL, Slack RS: **Role of AIF in caspase-dependent and caspase-independent cell death.** *Oncogene* 2004, **23**:2785–2796.
35. Hong SJ, Dawson TM, Dawson VL: **Nuclear and mitochondrial conversations in cell death: PARP-1 and AIF signaling.** *Trends Pharmacol Sci* 2004, **25**:259–264.
36. Menendez JA, Lupu R: **Fatty acid synthase and the lipogenic phenotype in cancer pathogenesis.** *Nat Rev Cancer* 2007, **7**:763–777.
37. Brusselmans K, De Schrijver E, Verhoeven G, Swinnen JV: **RNA interference-mediated silencing of the acetyl-CoA-carboxylase-alpha gene induces growth inhibition and apoptosis of prostate cancer cells.** *Cancer Res* 2005, **65**:6719–6725.
38. Chajes V, Cambot M, Moreau K, Lenoir GM, Joulin V: **Acetyl-CoA carboxylase alpha is essential to breast cancer cell survival.** *Cancer Res* 2006, **66**:5287–5294.
39. Wang C, Xu C, Sun M, Luo D, Liao DF, Cao D: **Acetyl-CoA carboxylase-alpha inhibitor TOFA induces human cancer cell apoptosis.** *Biochem Biophys Res Commun* 2009, **385**:302–306.
40. Beckers A, Organe S, Timmermans L, Scheys K, Peeters A, Brusselmans K, Verhoeven G, Swinnen JV: **Chemical inhibition of acetyl-CoA carboxylase induces growth arrest and cytotoxicity selectively in cancer cells.** *Cancer Res* 2007, **67**:8180–8187.
41. Milgraum LZ, Witters LA, Pasternack GR, Kuhajda FP: **Enzymes of the fatty acid synthesis pathway are highly expressed in in situ breast carcinoma.** *Clin Cancer Res* 1997, **3**:2115–2120.
42. Swinnen JV, Vanderhoydonc F, Elgamal AA, Eelen M, Vercaeren I, Joniau S, Van Poppel H, Baert L, Goossens K, Heyns W, *et al*: **Selective activation of the fatty acid synthesis pathway in human prostate cancer.** *Int J Cancer* 2000, **88**:176–179.
43. Chang C-C, Lin C-J: **LIBSVM: A library for support vector machines.** *ACM Trans Intell Syst Technol* 2011, **2**:1–27.
44. Kaida D, Motoyoshi H, Tashiro E, Nojima T, Hagiwara M, Ishigami K, Watanabe H, Kitahara T, Yoshida T, Nakajima H, *et al*: **Spliceostatin A targets SF3b and inhibits both splicing and nuclear retention of pre-mRNA.** *Nat Chem Biol* 2007, **3**:576–583.
45. Natsume T, Yamauchi Y, Nakayama H, Shinkawa T, Yanagida M, Takahashi N, Isobe T: **A direct nanoflow liquid chromatography-tandem mass spectrometry system for interaction proteomics.** *Anal Chem* 2002, **74**:4725–4733.
46. Tornøe CW, Chirstensen C, Meldal MJ: *Org Chem* 2002, **67**:3057–3064.
47. Rostovtsev VV, Green LG, Fokin VV, Sharpless KB: *Angew Chem Int Ed* 2002, **41**:2596–2599.

doi:10.1186/1472-6769-12-2
Cite this article as: Kobayashi *et al.*: **Comprehensive predictions of target proteins based on protein-chemical interaction using virtual screening and experimental verifications.** *BMC Chemical Biology* 2012 **12**:2.

U7 small nuclear ribonucleoprotein represses histone gene transcription in cell cycle-arrested cells

Takashi Ideue[a,1], Shungo Adachi[b], Takao Naganuma[a], Akie Tanigawa[a], Tohru Natsume[b], and Tetsuro Hirose[a,2]

[a]Functional RNomics Team and [b]Biological Systems Control Team, Biomedicinal Information Research Center, National Institute of Advanced Industrial Science and Technology (AIST), Koutou, Tokyo 135-0064, Japan

Edited by James L. Manley, Columbia University, New York, NY, and approved February 29, 2012 (received for review January 11, 2012)

Histone gene expression is tightly coordinated with DNA replication, as it is activated at the onset of S phase and suppressed at the end of S phase. Replication-dependent histone gene expression is precisely controlled at both transcriptional and posttranscriptional levels. U7 small nuclear ribonucleoprotein (U7 snRNP) is involved in the 3′-end processing of nonpolyadenylated histone mRNAs, which is required for S phase-specific gene expression. The present study reports a unique function of U7 snRNP in the repression of histone gene transcription under cell cycle-arrested conditions. Elimination of U7 snRNA with an antisense oligonucleotide in HeLa cells as well as in nontransformed human lung fibroblasts resulted in elevated levels of replication-dependent H1, H2A, H2B, H3, and H4 histone mRNAs but not of replication-independent H3F3B histone mRNA. An analogous effect was observed upon depletion of Lsm10, a component of the U7 snRNP-specific Sm ring, with siRNA. Pulse–chase experiments revealed that U7 snRNP acts to repress transcription without remarkably altering mRNA stability. Mass spectrometric analysis of the captured U7 snRNP from HeLa cell extracts identified heterogeneous nuclear (hn)RNP UL1 as a U7 snRNP interaction partner. Further knockdown and overexpression experiments revealed that hnRNP UL1 is responsible for U7 snRNP-dependent transcriptional repression of replication-dependent histone genes. Chromatin immunoprecipitation confirmed that hnRNP UL1 is recruited to the histone gene locus only when U7 snRNP is present. These findings support a unique mechanism of snRNP-mediated transcriptional control that restricts histone synthesis to S phase, thereby preventing the potentially toxic effects of histone synthesis at other times in the cell cycle.

RNA regulator | RNA-binding protein | RNP pulldown

In eukaryotic cells, sufficient histones must be synthesized in concert with DNA replication to package the newly replicated DNA into chromatin. The expression of replication-dependent histone genes, which encode five core histone species (H1, H2A, H2B, H3, and H4), is highly stimulated at the beginning of S phase and sharply suppressed at the end of S phase in metazoans (1). The expression of replication-dependent histone genes is coordinately activated at the transcription level at the G1/S-phase transition. The cyclin E-Cdk2 substrate p220/NPAT reportedly plays an essential role in the coordinate transcriptional activation of histone genes at the onset of S phase (2, 3). Through its direct interaction with subtype-specific transcription factors such as HiNF-P, which is required for histone H4 promoter activation (4), p220/NPAT activates histone gene transcription. The active transcription of histone genes requires ongoing DNA replication; therefore, the arrest of DNA replication with hydroxyurea or DNA damage induced by ionizing radiation leads to rapid transcriptional suppression (5, 6).

Replication-dependent histone genes produce nonpolyadenylated mRNAs that possess a conserved stem-loop (SL) structure (1, 7, 8). The noncanonical structure of the 3′ terminus of histone mRNAs significantly contributes to S phase-specific histone gene expression. Nonpolyadenylated histone mRNAs are synthesized as a consequence of the unique 3′ processing mechanism. Endonucleolytic cleavage occurs between two sequence elements, including a conserved SL structure and a purine-rich histone downstream element (HDE) that are separated by ~15 nt (8–10).

The HDE interacts with the U7 small nuclear ribonucleoprotein (snRNP), which is composed of U7 snRNA and an Sm ring. The Sm ring of U7 snRNP differs from that in spliceosomal snRNPs, containing Lsm10 and Lsm11 in place of SmD1 and SmD2 (11, 12). U7 snRNP is recruited to histone pre-mRNA primarily through base-pair formation between the 5′ end of U7 snRNA and the HDE (8, 10). The SL structure is associated with the SL-binding protein (SLBP) (13), and it stabilizes the binding of U7 snRNP to histone pre-mRNAs (14).

SLBP binds a 100-kDa zinc finger protein (ZFP100) that interacts with Lsm11 (15). SLBP is the limiting factor for S phase-specific histone mRNA synthesis (16). In mammalian cells, SLBP synthesis is activated just before entry into S phase, and phosphorylation of a specific threonine in SLBP by cyclin A/Cdk1 triggers rapid degradation at the end of S phase (16, 17). SLBP degradation leads to the destabilization of histone mRNAs, which prompts the rapid shutoff of histone gene expression at the end of S phase. Factors involved in the transcription and mRNA processing of histone genes (e.g., NPAT) are commonly localized to distinct nuclear foci, called histone locus bodies (HLBs), near the chromosomal loci of histone gene clusters. The HLBs often overlap with or are located in close proximity to the Cajal body, a classical nuclear body detected during the immunostaining of coilin (8, 18, 19).

We recently reported that the efficient depletion of U7 snRNA in HeLa cells with an antisense oligonucleotide (ASO) leads to a defect in the 3′-end processing of histone mRNAs and a concomitant delay in S-phase progression (20). Cell-cycle progression was arrested at the transition step between G1 and S phase (G1/S) using a double-thymidine block for cell synchronization, and the arrested cells were used for U7 snRNA depletion. Unexpectedly, processed histone mRNAs accumulated at elevated levels, even in the absence of U7 snRNA, under cell cycle-arrested conditions. This discovery raised the intriguing possibility that U7 snRNA can suppress histone gene expression under cell cycle-arrested conditions.

In this paper, we report a unique function of U7 snRNA in histone gene expression in which U7 snRNA acts to repress transcription of replication-dependent histone genes during cell-cycle arrest. We identified heterogeneous nuclear (hn)RNP UL1 as the U7 snRNP interactor that is responsible for the repression. These data reveal dual roles of U7 snRNPs that strictly regulate histone gene expression to prevent the production of extra histones, which are harmful to the cell.

Author contributions: T.I. and T.H. designed research; T.I., S.A., T. Naganuma, A.T., and T.H. performed research; S.A. and T. Natsume contributed new reagents/analytic tools; T.I., S.A., and T.H. analyzed data; and T.H. wrote the paper.

The authors declare no conflict of interest.

This article is a PNAS Direct Submission.

[1]Present address: Department of Biological Sciences, Graduate School of Science and Technology, Kumamoto University, Kumamoto 860-8555, Japan.

[2]To whom correspondence should be addressed. E-mail: tets-hirose@aist.go.jp.

This article contains supporting information online at www.pnas.org/lookup/suppl/doi:10.1073/pnas.1200523109/-/DCSupplemental.

BIOCHEMISTRY

Results

Elimination of U7 snRNA Leads to the Up-Regulation of Histone Gene Expression in Cell Cycle-Arrested Cells. U7 snRNA was eliminated with the ASO in HeLa cells in which the cell cycle was arrested at G1/S phase using a double-thymidine block (ΔU7 cells) (lane ΔU7 in Fig. 1*A*). When the cell cycle-arrested period was extended for 24 or 48 h by culturing the cells in thymidine-containing media, the accumulation of matured histone H1C mRNA in ΔU7 cells was markedly elevated (eightfold) compared with accumulation in control cells (open circle in Fig. 1*D*). Similar up-regulation was detected in other subclasses of histone mRNAs (H1–H4) but not in H3F3B, a replication-independent histone gene that produces polyadenylated mRNA (21) (Fig. 1*C*). Elimination of U7 snRNA caused neither aberrant cell-cycle entry into S phase (Fig. 1*B* and Fig. S1*A*) nor aberrant amplification of histone gene copy number (Fig. S1*B*) during extended cell-cycle arrest.

The elevation of H1 mRNA detected by quantitative (q)RT-PCR was not caused by the aberrant synthesis of polyadenylated histone mRNAs in ΔU7 cells. This conclusion is evidenced by the fact that most of the increased band in the Northern blot corresponded to processed mRNAs (Fig. 1*D*), which were not captured by oligo(dT) selection (Fig. 1*E*). Moreover, qRT-PCR detected the marked increase of histone mRNA levels in the nonpolyadenylated RNA fraction (oligo dT-sups in Fig. 1*F*). Marked elevation of mRNA levels of the replication-dependent histone genes upon U7 snRNA depletion was observed in quiescent nontransformed fibroblasts (MRC5) (Fig. S2 *A–C*), indicating that the effect is not restricted to the transformed cell lines. Furthermore, when ΔU7 cells were semisynchronized with nocodazole (which arrested the cell cycle at M phase) and the cell cycle was subsequently reinitiated by the removal of nocodazole, the levels of histone mRNAs were also elevated after 8 h (Fig. S2 *D* and *E*). In contrast, a threefold up-regulation of U7 snRNA by expression from the transfected plasmid in the cell cycle-arrested cells (lane U7 in Fig. 1*A*) led to the down-regulation of five replication-dependent histone genes but not of the replication-independent H3F3B gene (Fig. 1*G*).

At the onset of S phase triggered by thymidine removal, the stimulation of histone gene expression was observed in both control and ΔU7 cells, although the elevation of mRNA levels was less remarkable in ΔU7 cells (Fig. S3). This observation indicates that the S phase-specific activation of histone gene expression per se is poorly affected by the status of cellular U7 snRNA. The higher accumulation of histone mRNAs in ΔU7 cells at S phase was likely caused by elevation of basal accumulation levels at G1/S phase. These data argue that U7 snRNA acts to repress histone gene expression under cell cycle-arrested conditions.

To exclude the possibility that the ASO for U7 snRNA knockdown artificially increased histone mRNA levels, a protein component of U7 snRNP (Lsm10) was eliminated with siRNA. U7 snRNA was obliterated in ΔLsm10 cells (Fig. 1*H*). Elevated accumulations of processed histone H1C mRNA and the aberrantly polyadenylated form were detected in ΔLsm10 cells (Fig. 1*H*). This result supports our observations in ΔU7 cells and also

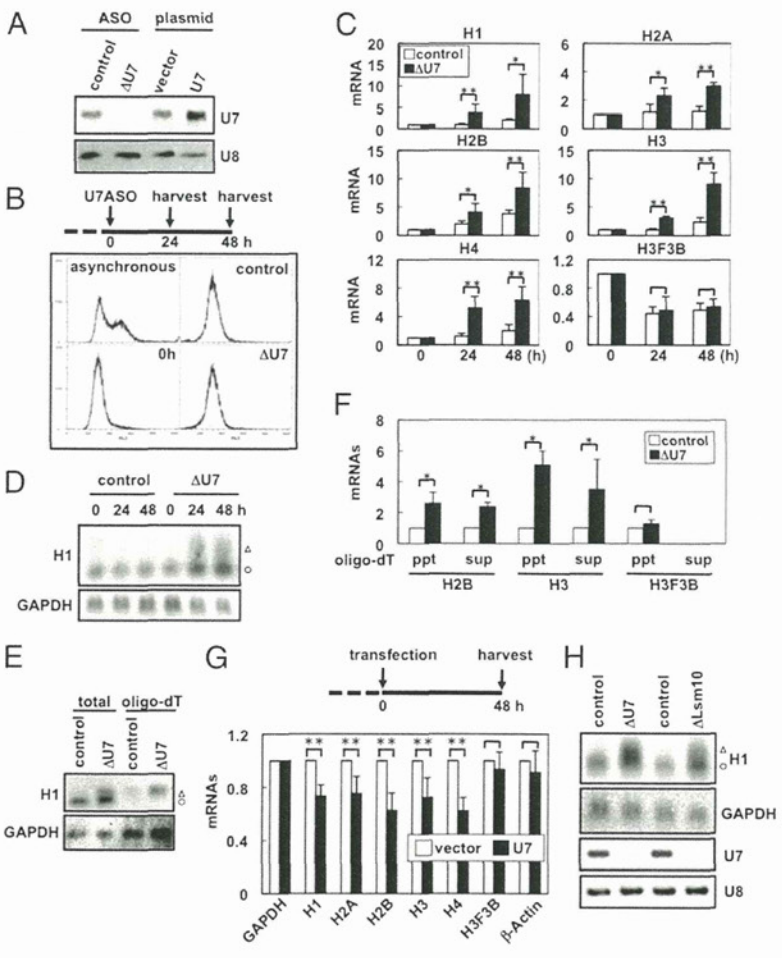

Fig. 1. U7 snRNA acts to repress histone gene expression during cell-cycle arrest. (*A*) Manipulation of the intracellular level of U7 snRNA. Obliteration of U7 snRNA with knockdown with ASO (lane ΔU7) and elevation of U7 snRNA level by expression from the transfected plasmid (lane U7) were confirmed by Northern blot analysis. U8 is the control RNA. (*B*) Experimental time schedule of U7 ASO administration (U7 ASO) and cell harvest (harvest) is shown above. The dashed line indicates the period of cell synchronization by the addition of excess thymidine. After ASO administration, cells were cultured in thymidine-containing medium until harvest (solid line). Cell-cycle profiles of asynchronous cells and synchronized cells before (0 h) or after administration of GFP-ASO (control) or U7 ASO (ΔU7) were monitored by FACS analysis. (*C*) Quantitative RT-PCR to measure the levels of histone mRNAs (H1, H2A, H2B, H3, and H4) upon elimination of U7 snRNA (black bars). Levels in control cells (white bars) at 0 h are adjusted to 1.0. H3F3B is the control mRNA. (*D* and *E*) Northern blot analysis to detect histone H1C after elimination of U7 snRNA (ΔU7). Open triangles and circles represent aberrantly polyadenylated and normally processed H1C mRNAs, respectively, which were identified by Northern blot with oligo-dT–selected RNAs (*E*). GAPDH is the control mRNA. (*F*) Quantitative RT-PCR to measure the levels of polyadenylated (oligo-dT ppt) and nonpolyadenylated (oligo-dT sup) histone mRNAs upon elimination of U7 snRNA (black bars) (*$P < 0.1$, Student's *t* test). (*G*) The time schedule of the experiment is shown above. Histone mRNA levels in vector-transfected cells (white bars) and U7 snRNA-transfected cells (black bars) were measured by qRT-PCR. Levels in the vector-transfected cells are adjusted to 1.0. Control mRNAs are GAPDH, H3F3B, and β-actin (**$P < 0.01$, Student's *t* test). (*H*) U7 snRNP suppresses the expression of H1C mRNA. Northern blot analysis was performed to detect H1C mRNA and U7 snRNA in Lsm10-eliminated cells with siRNA (ΔLsm10). Aberrantly polyadenylated and normally processed H1C mRNAs are represented as in *D*. GAPDH and U8 are control RNAs.

indicates that U7 snRNA acts as a canonical U7 snRNP with the Sm ring for the repression of histone gene expression.

U7 snRNP Represses the Transcription of Histone Genes. To clarify the step(s) that U7 snRNP suppresses, the levels of newly synthesized nascent histone mRNAs were measured in cell cycle-arrested ΔU7 cells and control cells. The uridine analog 5-ethynyl uridine (EU) was incorporated into cells cultured in thymidine-containing medium for 30 min, after which EU-containing nascent RNAs were captured. Quantitative RT-PCR revealed that the levels of the captured nascent mRNAs for five histone genes, but not the GAPDH gene, were markedly increased in ΔU7 cells (Fig. 2*A*). This finding indicates that the transcription of histone genes was stimulated by U7 snRNA depletion. We confirmed that the U7 snRNA depletion reduced or did not affect the stability of histone mRNAs by measuring the half-lives of EU pulse-labeled histone mRNAs (Fig. 2*B*) and unlabeled histone mRNAs after treatment with a transcription inhibitor, actinomycin D (Fig. 2*C*). Northern blot analysis showed that the processed forms comprised most of the accumulated H3 mRNA in ΔU7 cells (open circle in Fig. 2*C*), and the stability of the processed H3 mRNAs was even lower in ΔU7 cells (Fig. 2*C*). The processed H3 mRNA was confirmed to be nonpolyadenylated (Fig. S4*A*) and accurately processed at the 3′ terminus, which was identical to the position in control cells (Fig. S4*B*). These results indicate that the elimination of U7 snRNA leads to transcriptional derepression of replication-dependent histone genes, with neither stabilization of histone mRNAs nor alteration of mRNA processing accuracy. We further investigated whether U7 snRNP modulates transcription from histone gene promoters using the firefly luciferase (FFluc) reporter driven by the H1C promoter. Because this construct produces canonically polyadenylated FFluc mRNA, the role of U7 snRNP in transcription could be separated from its role in mRNA processing. As shown in Fig. 2*D*, the H1C promoter was significantly up-regulated upon depletion of U7 snRNA (*Left*), whereas it was slightly down-regulated in cells overexpressing U7 (*Right*), indicating that U7 snRNP can repress transcription from the H1C promoter.

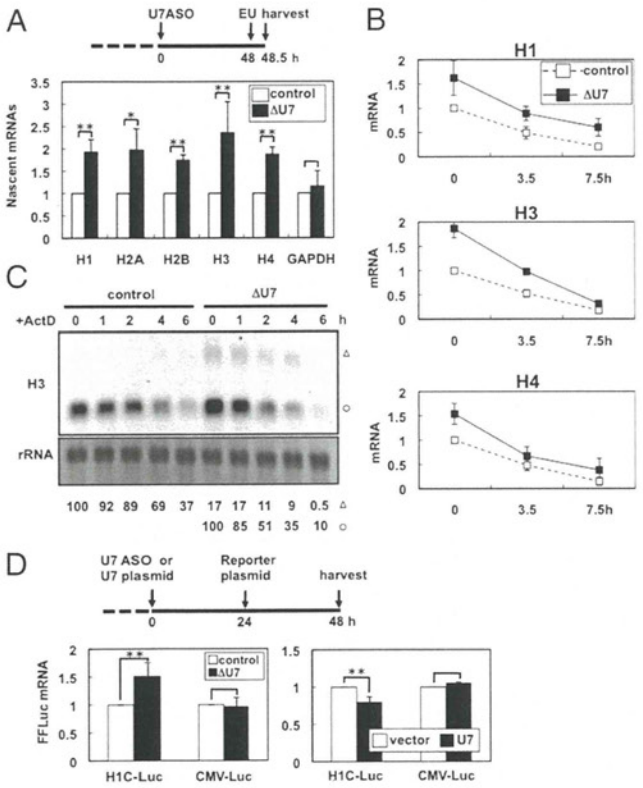

Fig. 2. U7 snRNP represses transcription of histone mRNAs. (*A*) Quantification of nascent histone mRNAs in control cells (white bars) and ΔU7 cells (black bars). EU-labeled mRNAs were quantified by qRT-PCR (*$P < 0.1$, **$P < 0.01$, Student's *t* test). The experimental time schedule is shown as in Fig. 1*B*. (*B*) Quantification of the stability of histone mRNAs. The degradation of pulse-labeled mRNAs was quantified in chased cells by qRT-PCR. (*C*) Northern blot analysis was performed to monitor the degradation of histone H3 mRNA. RNA samples were prepared from control or ΔU7 cells at different time points (0–6 h) after the addition of actinomycin D. Aberrantly polyadenylated and normally processed H3 mRNAs are represented as in Fig. 1*D*. Control RNA is 18S rRNA. (*D*) Effects of depletion and overexpression of U7 snRNA on H1C promoter activity. H1C promoter-Luc reporter (H1C-Luc) or CMV promoter-Luc reporter (CMV-Luc) was transfected into control cells or ΔU7 cells (*Left*) or into control cells or cells overexpressing U7 (*Right*). The normalized FFluc mRNA levels are plotted (**$P < 0.01$, Student's *t* test). The time schedule is the same as that shown in Fig. 1*B*.

hnRNP UL1 Is an Interactor of U7 snRNP. Known U7 snRNP-interacting proteins have been limited to factors involved in the 3′-end processing of histone mRNAs. Therefore, we attempted to capture U7 snRNP with the ASO to identify the responsible factor(s) for the unique function of U7 snRNP in transcriptional repression. The established method for U7 snRNP purification (22) was subjected to an antisense 2′-*O*-methyl oligonucleotide. The identities of the proteins that were contained in the captured U7 snRNP fraction from HeLa cells were determined by highly sensitive direct nanoflow liquid chromatography/tandem mass spectrometry (LC-MS) (23). To exclude various proteins that are nonspecifically copurified in this procedure, three control experiments were applied: (*i*) pull down with only beads that are not conjugated with ASOs ("no oligo" in Fig. 3*B*); (*ii*) pull down with beads that are conjugated with the ASO whose sequence was scrambled ("scrambled oligo" in Fig. 3*B*); and (*iii*) pull down with U7 ASO-conjugated beads in the presence of excess unconjugated U7 ASO ("U7ASO + excess oligo" in Fig. 3*B*).

Specific pull down of U7 snRNPs was confirmed by detection of U7 snRNA and Lsm11 with Northern and Western blots, respectively (Fig. 3*A*). The numbers of peptides identified by LC-MS analysis in the purposed experiment (U7ASO) were compared with those in the three control experiments (Fig. 3*B*). Among the 194 proteins detected by LC-MS analysis, most of the proteins were nonspecifically pulled down with beads, antibody, or ASO, because they appeared in the control experiments as well as in the purposed experiments. However, one protein (hnRNP UL1; also known as E1B-AP5) was specifically enriched in the fraction with U7 ASO (peptide number per analysis: 9.75) but not in the control experiments (peptide number per analysis: 0.17).

The interaction between hnRNP UL1 and U7 snRNP was confirmed by coimmunoprecipitation (co-IP) with an anti-hnRNP UL1 antibody (αUL1) and by pull down with U7 ASO (Fig. 3*C*). Northern blotting of coimmunoprecipitated RNAs with the αUL1 antibody revealed that U7 snRNA interacted with hnRNP UL1 (lane αUL1 in Fig. 3*C*, *Left*). Western blotting confirmed the coprecipitation of hnRNP UL1 during the capture of U7 snRNP with U7 ASO (lane U7 in Fig. 3*C*, *Right*). Reciprocal co-IP from HeLa cells transfected with Flag-Lsm11 revealed the interaction between hnRNP UL1 and Flag-Lsm11 in the presence of RNase A (Fig. 3*D*).

These data strongly suggest that hnRNP UL1 associates with U7 snRNP through protein–protein interactions with the U7-specific Sm ring or its associated factors. The protein hnRNP UL1 originally was identified as an interactor with adenovirus E1B-55K protein (24) and reportedly represses transcription from various promoters (25). These previous findings suggest the involvement of hnRNP UL1 in U7-mediated transcriptional repression.

BIOCHEMISTRY

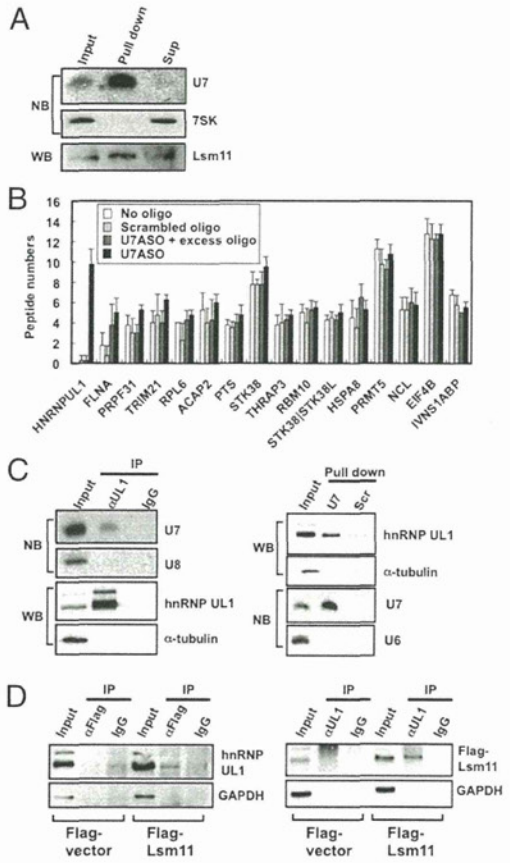

Fig. 3. Identification of hnRNP UL1 as a U7 snRNP component. (*A*) Purification of U7 snRNP. U7 snRNA and Lsm11 were detected in the purified U7 snRNP fraction (pull down) by Northern blot (NB) and Western blot (WB) analyses, respectively. (*B*) Detected proteins in the purified U7 snRNP fraction by LC-MS analysis. Black bars indicate the analyzed numbers of peptides from the proteins, whose peptides were read more than five times, in the purified U7 snRNA fraction with ASO (U7ASO). White, light gray, and dark gray bars indicate the analyzed numbers of peptides in the three control experiments (no oligo, scrambled oligo, and U7ASO+excess oligo, respectively). (*C*) hnRNP UL1 is a component of U7 snRNP. Immunoprecipitation with anti-hnRNP UL1 antibody (αUL1) and IgG as a control was performed. Pull down with U7 ASO (U7) and scrambled oligo (Scr) was performed. U7 snRNA was detected by Northern blot analysis and U6 or U8 snRNA was detected as a control. hnRNP UL1 was detected by Western blot and α-tubulin was detected as a control. (*D*) hnRNP UL1 interacts with Lsm11, a U7 snRNP protein. (*Left*) Immunoprecipitation with αFlag antibody in the presence of 10 μg/mL RNase A was carried out with an extract prepared from HeLa cells transfected with either the pcDNA-Flag vector (Flag-vector) or the Flag-Lsm11 expression plasmid (Flag-Lsm11). hnRNP UL1 was detected with the αUL1 antibody. (*Right*) Immunoprecipitation with the αUL1 antibody was performed as on the *Left*. Flag-Lsm11 was detected with an anti-Flag antibody. Input samples (2% starting material) were loaded onto "Input" lanes.

hnRNP UL1 Is Responsible for the Unique Function of U7 snRNP. To investigate the role of hnRNP UL1 in U7 snRNP, hnRNP UL1 was eliminated from cell cycle-arrested cells cultured in thymidine-containing medium with each of two siRNAs (ΔUL1-1 and ΔUL1-2 in Fig. 4*A*). The elimination did not affect cell-cycle arrest at G1/S phase (Fig. S1*A*), nor did it alter the accumulation level of U7 snRNA (Fig. 4*A*). This result was distinct from the effect of Lsm10 elimination, which destabilized U7 snRNA (Fig. 1*H*). The accumulation of replication-dependent histone mRNAs increased upon hnRNP UL1 elimination (Fig. 4 *B* and *C*). Importantly, Northern blotting showed that hnRNP UL1 elimination did not affect the 3′-end processing of H1C mRNA (lanes ΔUL1-1 and ΔUL1-2 in Fig. 4*B*), which was affected in ΔU7 and ΔLsm10 cells (Fig. 1 *D* and *H*). The overexpression of hnRNP UL1 from the transfected plasmid led to the down-regulation of histone gene expression (Fig. 4*D*). These data indicate that hnRNP UL1 is not involved in the 3′-end processing of histone mRNAs but is required for the repression of histone gene expression. Analysis of the captured nascent histone mRNAs revealed that hnRNP UL1 elimination mediated the increase in nascent histone mRNAs (Fig. 4*E*), which indicates that hnRNP UL1 can repress histone gene expression at the transcriptional level.

To examine whether hnRNP UL1 acts as part of U7 snRNP, the repression of histone gene expression by hnRNP UL1 was monitored in the presence or absence of U7 snRNA. The repression ($P < 0.05$) of H1 expression by hnRNP UL1 overexpression observed in control cells was less pronounced in ΔU7 cells (Fig. 4*F*). Additionally, when the repression of H2A expression by U7 snRNA was monitored in the presence or absence of hnRNP UL1, the repression of H2A expression ($P < 0.05$) by U7 snRNA overexpression observed in control cells was less pronounced in ΔUL1 cells (Fig. 4*G*). Although the degree of repression was weak due to experimental limitations, the above results suggest that hnRNP UL1 acts as a part of U7 snRNP to repress histone gene expression.

The recruitment of hnRNP UL1 to the histone gene locus was monitored by chromatin immunoprecipitation (ChIP) assay (Fig. 4*H*). Replication-dependent histone genes lack introns and, therefore, cover short genomic regions (*ca.* 700 bp). Accordingly, the chromatin was fragmented into smaller pieces (<500 bp) than those in the usual ChIP assay to discriminate each part of the histone gene. ChIP with the αUL1 antibody and subsequent detection of histone H2AA chromatin fragments revealed the association of hnRNP UL1 with the H2AA gene locus, with peak binding occurring near the terminator of the H2AA gene. Importantly, ChIP signals were markedly weakened in ΔU7 cells (ΔU7 in Fig. 4*H*), which indicates that hnRNP UL1 is recruited to the histone gene locus by association with U7 snRNP.

Discussion

The tight regulation of histone gene expression during each cell cycle is required to prevent harmful effects, such as genomic instability or hypersensitivity to DNA-damaging agents, due to the accumulation of the highly basic histones when DNA replication slows down or stops (26). Histone gene expression needs to be suppressed when the cell has passed the DNA-replication stage. We found that U7 snRNP represses histone gene expression under cell cycle-arrested conditions; this mechanism may help to prevent extra histone synthesis.

To investigate the impact of this mechanism, the levels of accumulated histones were analyzed in ΔU7 cells. Marked elevation of histone accumulation (approximately threefold) was observed when cells were treated with a proteasome inhibitor (Fig. S5). Without the treatment, histone levels were unchanged even if the levels of histone mRNAs were increased. The synthesis of extra histones from the increased mRNAs appears to be compensated by proteasome degradation in ΔU7 cells. These mechanisms of transcriptional repression and protein degradation may guarantee the prevention of extra histone synthesis. The repressive function of U7 snRNP was observed in quiescent nontransformed fibroblasts as well as in HeLa cells, suggesting that the U7 snRNP-mediated control of histone synthesis is a general regulatory mechanism adopted in various cell types.

Accurately processed histone mRNAs were detected at relatively high levels in ΔU7 cells. Although U7 snRNA depletion (to <5%) is likely to be sufficient to abolish the function of U7 snRNPs in ΔU7 cells, it cannot be ruled out that residual amounts of U7 snRNP are still able to process histone pre-mRNAs. A similar result was obtained under the condition of SLBP depletion, in which substantial levels of processed histone mRNAs

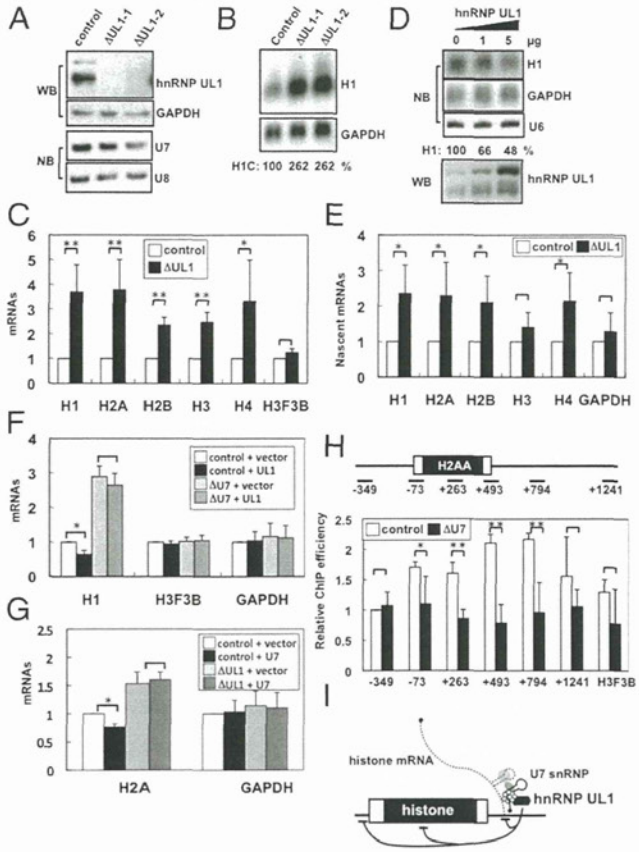

Fig. 4. hnRNP UL1 is the factor responsible for U7 snRNP function in the transcriptional repression of histone genes under cell cycle-arrested conditions. (*A*) Elimination of hnRNP UL1 does not affect U7 snRNA accumulation. hnRNP UL1 was treated with two siRNAs (ΔUL1-1 and ΔUL1-2) or control siRNA, and the elimination of hnRNP UL1 was confirmed by Western blot. U7 snRNA was detected in ΔUL1 cells by Northern blot. The siRNAs were administered into the cell cycle-arrested cells cultured in thymidine-containing medium. (*B*) hnRNP UL1 is not involved in the 3′-end processing of histone mRNAs but is involved in the repression of histone gene expression. Histone H1C mRNA in ΔUL1-1 and control cells was detected by Northern blot. H1C mRNA in ΔU7 cells is shown as the reference for the 3′-end processing defect. Aberrantly polyadenylated and normally processed H1C mRNAs are represented as in Fig. 1*D*. (*C*) Effects of hnRNP UL1 elimination with siRNA on histone mRNAs. Histone mRNA levels in ΔUL1-1 and control cells were quantified by qRT-PCR. (*D*) Overexpression of hnRNP UL1 suppresses histone H1C gene expression. The level of hnRNP UL1 in cells transfected with the expression plasmid was detected by Western blot. The plasmid amounts transfected are shown above the panel. The H1C level in hnRNP UL1-overexpressing cells was detected by Northern blotting. The quantified H1C level (normalized by GAPDH mRNA) is shown below the panel. (*E*) hnRNP UL1 represses the transcription of histone genes. Nascent histone mRNA levels in ΔUL1-1 and control cells were quantified by qRT-PCR. (*F*) Repression activity of hnRNP UL1 depends on the presence of U7 snRNA. H1 mRNA was quantified by qRT-PCR by using RNA samples prepared from control and ΔU7 cells transfected with either the control vector (vector) or the hnRNP UL1 expression plasmid (UL1). (*G*) Repression activity of U7 snRNA depends on the presence of hnRNP UL1. H2A mRNA was quantified by qRT-PCR by using RNA samples prepared from control and ΔhnRNP UL1 cells (ΔUL1) transfected with either the control vector (vector) or the U7 snRNA expression plasmid (U7). (*H*) ChIP of histone H2AA gene with anti-hnRNP UL1 antibody. Positions of the PCR primers used are shown above the panel. The H2AA mRNA region is boxed. ChIP levels from control or ΔU7 cells are indicated by white or black bars, respectively. $*P < 0.1$, $**P < 0.01$, Student's *t* test. (*I*) Model of U7 snRNP functions in histone gene expression. The curved lines below represent the repression of some steps of transcription.

accumulate in the cell (27). Another intriguing possibility is that an unidentified mechanism compensates for the 3′-end processing of histone mRNAs once a critical factor is abolished.

hnRNP UL1, the U7 snRNP-interacting protein, was recruited to the chromosomal locus of histone genes in cell cycle-arrested cells (Fig. 4*H*). The immunostaining results indicated that HLBs marked by NPAT were present in hnRNP UL1-localized nuclear foci in ∼15% of the cell population (Fig. S6). hnRNP UL1 has been shown to aid in transcriptional repression from various promoters, including the histone H2A promoter (25). This is consistent with the reporter assay results, which showed that U7 snRNP repressed transcription from the histone H1C promoter (Fig. 2*D*). The ChIP assay results revealed that the major association site of hnRNP UL1 was located near the transcription terminator of the histone H2AA gene, and that the association depended on U7 snRNA (Fig. 4*H*). These results suggest that hnRNP UL1 associates with U7 snRNP that binds to the nascent histone pre-mRNA, which may facilitate transcriptional repression of the cognate histone gene (Fig. 4*I*). Our data also suggest that the role of U7 snRNP in repression of histone gene transcription is distinct from the possible role of U7 snRNA in transcriptional control of the MDR1 gene, through interaction with the transcription factor NF-Y that binds to the MDR1 promoter (28). However, elucidation of the detailed mechanism by which hnRNP UL1 and U7 snRNP act to repress transcription will require further analysis.

The rapid transcriptional suppression of histone genes upon hydroxyurea treatment in S phase occurred properly in ΔU7 cells (Fig. S3), which indicates that the U7-mediated repression mechanism is distinct from the previously noted mechanism through the p53/p21-dependent pathway (6). Transcriptional activation of histone genes at the onset of S phase occurred normally in ΔU7 cells, which indicates that the U7-mediated repression does not affect the p220/NPAT-mediated transcriptional activation in S phase. However, how the two functions of U7 snRNP are switched depending on the cell-cycle phase remains unclear.

We have confirmed that hnRNP UL1 is associated with U7 snRNP in S phase, which indicates that the binding of hnRNP UL1 to U7 snRNP is unlikely to be the step that establishes the mode of action. Endonucleolytic cleavage to create the 3′ end of histone mRNAs is known to liberate the U7 snRNP that is used for the next round of processing (29). This observation suggests that the active transcription of histone genes in S phase facilitates the rapid turnover of U7 snRNP on the histone locus and thereby prevents hnRNP UL1 from playing a repressive function. Further mechanistic investigations regarding the role of U7 snRNP should provide unique insights into the multilayer regulatory system that maintains histone levels during each cell cycle.

Materials and Methods

Reagents and Molecular Biological Protocols. The chemicals used were purchased from Nacalai Tesque unless otherwise stated. See *SI Materials and Methods* for additional information.

Plasmid Construction and Transfection. The expression plasmid of U7 snRNA was cloned into the pGEM-T Easy Vector (Promega). The expression plasmid of Flag-Lsm11 was cloned into the pcDNA3-Flag vector (20). The expression plasmid of hnRNP UL1 was a gift from R. J. A. Grand (University of Birmingham, Birmingham, UK). The plasmid was administered into HeLa cells with Lipofectamine 2000 (Invitrogen) or by nucleofection with the Nucleofector device (Lonza) in accordance with the manufacturers' instructions.

Oligonucleotide Administration into Cells. The chemically modified chimeric ASO was synthesized and administered into synchronized HeLa cells with the Nucleofector device, as described previously (20). For RNAi, HeLa cells were transfected with siRNAs at 200 nM (final concentration) with the Nucleofector device in accordance with the manufacturer's instructions. Negative control siRNA was purchased from Invitrogen. Knockdown efficiencies were verified by immunoblotting or by qRT-PCR (30). The sequences of siRNAs,

BIOCHEMISTRY

ASOs, and primers for the qRT-PCR used in this study are listed in Tables S2, S3, and S4, respectively.

Cell Culture. HeLa cells were synchronized using a double-thymidine block (31). Thymidine (2.5 mM) was added to the culture medium, incubated for 18 h, and removed. The cells were then incubated without thymidine for 10 h. A second dose of thymidine (2.5 mM) was added, and the cells were incubated for 16 h (dashed line in Figs. 1 *B* and *G* and 2 *A* and *D* and Figs. S2*D* and S3). Synchronized cells at G1/S phase were used for administration of nucleic acids (ASO, siRNA, and/or plasmid). The nucleic acid-treated cells were further cultured in DMEM containing 2.5 mM thymidine (bold line in Figs. 1 *B* and *G* and 2 *A* and *D* and Figs. S2*D* and S3). MRC5 cells were cultured in αMEM with 10% (vol/vol) FBS. The medium was exchanged with serum-free αMEM 24 h before ASO administration. The ASO-treated MRC5 cells were cultured in serum-free medium for 48 h. The cells were processed for FACS analysis of cell-cycle distribution by measuring BrdU incorporation with the FITC BrdU Flow Kit (BD Sciences) and for DNA content with 7-amino-actinomycin D (7-AAD) or DAPI staining. FACS data were analyzed by Cell Lab Quanta SC software (Beckman Coulter).

Capture of Nascent RNAs. To capture nascent RNAs, 0.5 mM EU was incorporated into the cells for 30 min. EU-labeled RNAs were biotinylated and captured by using the Click-iT Nascent RNA Capture Kit (Invitrogen) in accordance with the manufacturer's instructions.

Immunoprecipitation and Pull Down of Ribonucleoprotein Complex. HeLa cells (1×10^6) were lysed with lysis buffer (50 mM Tris·HCl, pH 7.5, 150 mM NaCl, 50 mM NaF, 1 mM Na_3VO_4, 0.5% Nonidet P-40) for 30 min on ice, and the cell extract (1 μg protein) was used for immunoprecipitation and pull-down experiments. For IP, protein complexes were precipitated with an antibody against hnRNP UL1 conjugated to Dynabeads–protein G (Invitrogen) for 1 h at room temperature. The IP products were washed four times with lysis buffer. Detailed information about the antibodies used is shown in Table S1. The pull down of U7 snRNP was carried out by using ASO as described (22). Biotinylated antisense 2′-*O*-methyl oligonucleotide was synthesized by IDT. The ASO (400 pmol) was conjugated to Dynabeads–streptavidin T1 (Invitrogen) for 1 h in binding buffer (10 mM Tris·HCl, pH 7.5, 1 mM EDTA, 2 M NaCl, 0.1% Tween 20). The ASO–Dynabeads conjugates were incubated with cell extract for 1 h at 4 °C. The captured ribonucleoprotein complexes were then washed four times with lysis buffer. The identities of the captured proteins were determined by LC-MS (23). Detailed information about the ASO sequences used is shown in Table S3.

ACKNOWLEDGMENTS. We thank R. J. A. Grand for providing the hnRNP UL1 plasmid and members of the T.H. laboratory for valuable discussions and assistance. This research was supported by the Funding Program for Next Generation World-Leading Researchers (NEXT Program) of the Japan Society for the Promotion of Science; grants from the Ministry of Education, Culture, Sports, Science and Technology of Japan; the New Energy and Industrial Technology Development Organization; the Astellas Foundation for Research on Metabolic Disorders; and the Takeda Science Foundation.

1. Marzluff WF, Wagner EJ, Duronio RJ (2008) Metabolism and regulation of canonical histone mRNAs: Life without a poly(A) tail. *Nat Rev Genet* 9:843–854.
2. Ma T, et al. (2000) Cell cycle-regulated phosphorylation of p220(NPAT) by cyclin E/Cdk2 in Cajal bodies promotes histone gene transcription. *Genes Dev* 14:2298–2313.
3. Zhao J, et al. (2000) NPAT links cyclin E-Cdk2 to the regulation of replication-dependent histone gene transcription. *Genes Dev* 14:2283–2297.
4. Miele A, et al. (2005) HiNF-P directly links the cyclin E/CDK2/p220NPAT pathway to histone H4 gene regulation at the G1/S phase cell cycle transition. *Mol Cell Biol* 25:6140–6153.
5. Sittman DB, Graves RA, Marzluff WF (1983) Histone mRNA concentrations are regulated at the level of transcription and mRNA degradation. *Proc Natl Acad Sci USA* 80:1849–1853.
6. Su C, et al. (2004) DNA damage induces downregulation of histone gene expression through the G1 checkpoint pathway. *EMBO J* 23:1133–1143.
7. Osley MA (1991) The regulation of histone synthesis in the cell cycle. *Annu Rev Biochem* 60:827–861.
8. Marzluff WF (2005) Metazoan replication-dependent histone mRNAs: A distinct set of RNA polymerase II transcripts. *Curr Opin Cell Biol* 17:274–280.
9. Dominski Z, Marzluff WF (1999) Formation of the 3′ end of histone mRNA. *Gene* 239(1):1–14.
10. Tycowski KT, Kolev NG, Conrad NK, Fok V, Steitz JA (2006) *The RNA World*, eds Gesteland RF, Cech TR, Atkins JF (Cold Spring Harbor Lab Press, Cold Spring Harbor, NY), 3rd Ed, pp 327–368.
11. Pillai RS, Will CL, Lührmann R, Schümperli D, Müller B (2001) Purified U7 snRNPs lack the Sm proteins D1 and D2 but contain Lsm10, a new 14 kDa Sm D1-like protein. *EMBO J* 20:5470–5479.
12. Pillai RS, et al. (2003) Unique Sm core structure of U7 snRNPs: Assembly by a specialized SMN complex and the role of a new component, Lsm11, in histone RNA processing. *Genes Dev* 17:2321–2333.
13. Wang ZF, Whitfield ML, Ingledue, TC, III, Dominski Z, Marzluff WF (1996) The protein that binds the 3′ end of histone mRNA: A novel RNA-binding protein required for histone pre-mRNA processing. *Genes Dev* 10:3028–3040.
14. Dominski Z, Zheng LX, Sànchez R, Marzluff WF (1999) Stem-loop binding protein facilitates 3′-end formation by stabilizing U7 snRNP binding to histone pre-mRNA. *Mol Cell Biol* 19:3561–3570.
15. Dominski Z, Erkmann JA, Yang X, Sànchez R, Marzluff WF (2002) A novel zinc finger protein is associated with U7 snRNP and interacts with the stem-loop binding protein in the histone pre-mRNP to stimulate 3′-end processing. *Genes Dev* 16(1):58–71.
16. Zheng L, et al. (2003) Phosphorylation of stem-loop binding protein (SLBP) on two threonines triggers degradation of SLBP, the sole cell cycle-regulated factor required for regulation of histone mRNA processing, at the end of S phase. *Mol Cell Biol* 23:1590–1601.
17. Koseoglu MM, Graves LM, Marzluff WF (2008) Phosphorylation of threonine 61 by cyclin a/Cdk1 triggers degradation of stem-loop binding protein at the end of S phase. *Mol Cell Biol* 28:4469–4479.
18. Frey MR, Matera AG (1995) Coiled bodies contain U7 small nuclear RNA and associate with specific DNA sequences in interphase human cells. *Proc Natl Acad Sci USA* 92:5915–5919.
19. Shopland LS, et al. (2001) Replication-dependent histone gene expression is related to Cajal body (CB) association but does not require sustained CB contact. *Mol Biol Cell* 12:565–576.
20. Ideue T, Hino K, Kitao S, Yokoi T, Hirose T (2009) Efficient oligonucleotide-mediated degradation of nuclear noncoding RNAs in mammalian cultured cells. *RNA* 15:1578–1587.
21. Albig W, et al. (1995) The human replacement histone H3.3B gene (H3F3B). *Genomics* 30:264–272.
22. Smith HO, et al. (1991) Two-step affinity purification of U7 small nuclear ribonucleoprotein particles using complementary biotinylated 2′-*O*-methyl oligoribonucleotides. *Proc Natl Acad Sci USA* 88:9784–9788.
23. Natsume T, et al. (2002) A direct nanoflow liquid chromatography-tandem mass spectrometry system for interaction proteomics. *Anal Chem* 74:4725–4733.
24. Gabler S, et al. (1998) E1B 55-kilodalton-associated protein: A cellular protein with RNA-binding activity implicated in nucleocytoplasmic transport of adenovirus and cellular mRNAs. *J Virol* 72:7960–7971.
25. Kzhyshkowska J, Rusch A, Wolf H, Dobner T (2003) Regulation of transcription by the heterogeneous nuclear ribonucleoprotein E1B-AP5 is mediated by complex formation with the novel bromodomain-containing protein BRD7. *Biochem J* 371:385–393.
26. Singh RK, Kabbaj MHM, Paik J, Gunjan A (2009) Histone levels are regulated by phosphorylation and ubiquitylation-dependent proteolysis. *Nat Cell Biol* 11:925–933.
27. Sullivan KD, Mullen TE, Marzluff WF, Wagner EJ (2009) Knockdown of SLBP results in nuclear retention of histone mRNA. *RNA* 15:459–472.
28. Higuchi T, Anzai K, Kobayashi S (2008) U7 snRNA acts as a transcriptional regulator interacting with an inverted CCAAT sequence-binding transcription factor NF-Y. *Biochim Biophys Acta* 1780:274–281.
29. Walther TN, Wittop Koning TH, Schümperli D, Müller B (1998) A 5′-3′ exonuclease activity involved in forming the 3′ products of histone pre-mRNA processing in vitro. *RNA* 4:1034–1046.
30. Sasaki YTF, Ideue T, Sano M, Mituyama T, Hirose T (2009) MENε/β noncoding RNAs are essential for structural integrity of nuclear paraspeckles. *Proc Natl Acad Sci USA* 106:2525–2530.
31. Whitfield ML, et al. (2000) Stem-loop binding protein, the protein that binds the 3′ end of histone mRNA, is cell cycle regulated by both translational and post-translational mechanisms. *Mol Cell Biol* 20:4188–4198.

Organic & Biomolecular Chemistry

Cite this: *Org. Biomol. Chem.*, 2012, **10**, 7826

www.rsc.org/obc

PAPER

Synthesis of vitamin D_3 derivatives with nitrogen-linked substituents at A-ring C-2 and evaluation of their vitamin D receptor-mediated transcriptional activity†

Junko Abe,[a] Yu Nagai,[a] Rui Higashikuni,[a] Keisuke Iida,[a] Takatsugu Hirokawa,[b] Hazuki Nagai,[c] Kaichiro Kominato,[c] Toshio Tsuchida,[c] Michiko Hirata,[a] Masaki Inada,[a] Chisato Miyaura[a] and Kazuo Nagasawa*[a]

Received 24th May 2012, Accepted 3rd August 2012
DOI: 10.1039/c2ob26017d

Binding of a series of novel 1α,25-dihydroxyvitamin D_3 (1,25-VD_3) derivatives, having a nitrogen-linked substituent at the 2α- or 2β-position of the A-ring (2-*N*-substituted compounds), with the vitamin D receptor (VDR) was investigated by means of computational docking studies. Selected compounds were synthesized by coupling A-ring synthons **6** and/or **7** with CD-ring-bearing bromomethylene **5** under Trost's conditions. The 2α- and 2β-stereoisomers of the A-ring synthons were synthesized from L-serine (**8**) as a single chiral source by installing vinyl and propargyl groups at opposite ends of the molecule. The activity of the obtained compounds was evaluated by means of a luciferase-based VDR transcriptional activity assay in NIH3T3 cells. Relatively small substituents incorporating a hydrogen-bonding donor, *i.e.*, NHAc and NHMs, were effective for eliciting VDR transcriptional activity, and 2β-NHMs-1,25-VD_3 (**Xa**) showed the highest activity, being more potent than 1,25-VD_3. Derivatives with bulky substituents were inactive. These new insights into the structure–activity relationships of 1,25-VD_3 derivatives may be helpful in separating the various biological activities of 1,25-VD_3 and in generating novel therapeutic drug candidates.

1. Introduction

1α,25-Dihydroxyvitamin D_3 (**1**) (1,25-VD_3) (Fig. 1), the active metabolite of vitamin D_3, plays central roles in various biological processes, acting *via* its specific receptor, *i.e.*, vitamin D receptor (VDR), which is a member of the nuclear receptor (NR) superfamily.[1] 1,25-VD_3 modulates bone metabolism,[2] cell proliferation and cell differentiation.[3] These characteristic biological activities deeply relate with various diseases, including osteoporosis, cancer, secondary hyperparathyroidism and psoriasis.[4] Since 1,25-VD_3 and related compounds are promising candidates for the treatment of these diseases, thousands of vitamin D derivatives have been synthesized in attempts to separate and/or enhance their biological activities,[5] and some of these compounds are in clinical use.[5a–c,e] In recent structure–activity relationship studies of vitamin D, much attention has been paid to modification of the A-ring.[5b,c,e,6] This ring contains the 1α- and 3β-hydroxyl groups, which have important interactions with VDR at Ser237 and Arg274 (for the 1α-hydroxyl group) and at Ser278 and Tyr143 (for the 3β-hydroxyl group), as determined by X-ray analysis.[10] The X-ray structure also indicated the presence of an unoccupied region in the binding site of VDR near the location of C2 of the A-ring of 1,25-VD_3. Therefore, introduction of substituents at C2 in the A-ring may alter the strength or the mode of interaction of the ligand with VDR, which may lead to conformational change of VDR, as well as changes in the characteristic biological activities. In fact, modification at the C2 position with oxygen- or carbon-containing groups has been intensively explored, and the resulting derivatives were reported to show characteristic and/or new biological activities.[7–9] For example, introduction of a 2α-hydroxypropyl[8] or 2α-methyl[9] group increased the binding affinity for VDR by 4- and 3-fold, respectively. These analogs also showed extremely high calcium-mobilizing activity, having 7 and 500 times higher potency than 1,25-VD_3 (**1**), respectively.[7] Further, introduction of a 2β-hydroxypropoxy group afforded a compound (ED-71; **2**) that appears to increase the bone mineral density in osteoporotic patients

[a]*Department of Biotechnology and Life Science, Faculty of Technology, Tokyo University of Agriculture and Technology, 2-24-16 Naka-cho, Koganei, Tokyo 184-8588, Japan. E-mail: knaga@cc.tuat.ac.jp; Fax: +81-42-388-7295; Tel: +81-42-388-7295*
[b]*National Institute of Advanced Industrial Science and Technology Tokyo Waterfront Bio-IT Research Building, 2-4-7 Aomi, Koto-ku, Tokyo, 135-0064, Japan*
[c]*MicroBiopharm Japan Co. 3-3-6 Nihonbashihoncho, Chuo-ku, Tokyo, 103-0032, Japan*
†Electronic supplementary information (ESI) available. See DOI: 10.1039/c2ob26017d

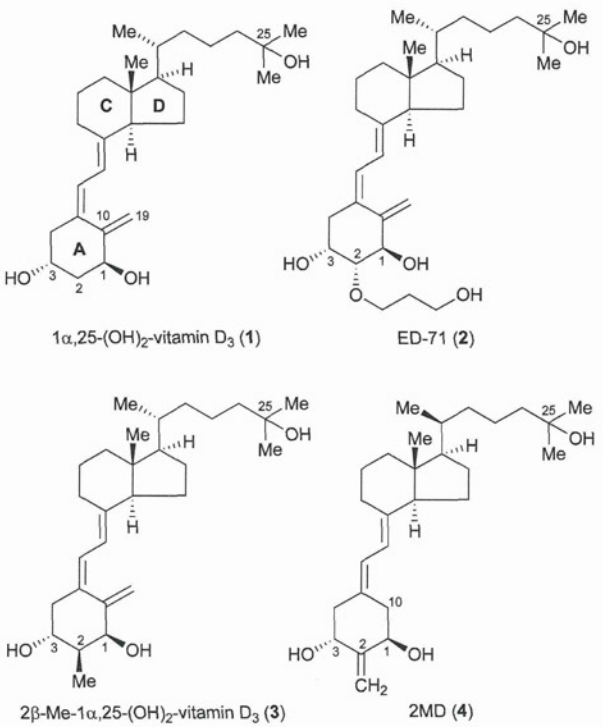

Fig. 1 Structures of 1α,25-dihydroxyvitamin D_3 and its synthetic analogs modified at the C2 position.

without significant side effects.[11] An analog of 2MD (**4**) having a methylene group at C2 also caused a bone mass increment without inducing hypercalcemia.[12] These results clearly show the potential of modifications at the C2 position in the A-ring of the vitamin D skeleton for eliciting a broad range of biological activities.

Here, we focused on installing nitrogen-linked functional groups at C2 in the A-ring to obtain 2-*N*-substituted compounds. Nitrogen has a different electrostatic field from oxygen or carbon, as well as a different number of substituents and different bond angles. Therefore, vitamin D derivatives with *N*-substituents at the C2 position can be expected to show different VDR-binding modes from the corresponding oxygen and/or carbon-substituted vitamin D derivatives, and so might have characteristically different biological activities.[13]

Firstly, we carried out docking studies of various 2-*N*-substituted vitamin D derivatives, **I** ~ **X** (Fig. 2), with the AF2 domain of VDR using the Glide (Schrödinger, LLC).[14,15] The docking scores are summarized in Table 1.[16]

In the case of 2α-*N*-monoalkyl groups (category **I**, **Ia–Ie**), higher stabilization was seen as the bulkiness increased from methyl to *n*-butyl group, but a remarkably low stabilization score was obtained for the *N*-benzyl-substituted derivative (**Ie**), probably because of steric hindrance. A similar trend was observed in the case of 2α-*N*,*N*′-dialkyl substitution (category **II**). The 2α-*N*,*N*′-diethyl-substituted derivative (**IIb**) was well docked with the AF2 domain (see Fig. 3(a)). Among the compounds in category **II**, no poses were obtained for the bulky *N*,*N*′-di-*n*-butyl- and *N*,*N*′-dibenzyl-substituted compounds (**IId** and **IIe**). Substitution of a 2α-*N*-amide group (category **III**) resulted in relatively low calculated affinity for VDR. The docking result for the 2α-*N*-benzoyl derivative (**IIIc**) is illustrated in Fig. 3(b). The sterically hindered phenyl group in **IIIc** reduces the stability as a result of steric interaction with Lys240 of VDR. Moderate stabilization scores were obtained for carbamate-substituted derivatives (category **IV**). The 2α-*N*-acyl and carbamate groups showed no significant interaction of their carbonyl groups with amino acid residues of VDR. In the case of 2α-*N*-sulfonamide substitution (category **V**), no poses were obtained except for the *N*-methanesulfonamide derivative **Va**. This compound **Va** was well docked with VDR (see Fig. 3(c)), and it showed greater stabilization than 1,25-VD_3.

The 2β-*N*-substituted derivatives (categories **VI–X**) showed similar trends to the case of 2α-*N*-substitution. 2β-*N*-monoalkyl groups (**VIa–d**), a 2β-*N*-acetyl group (**VIIIa**) and especially a *N*-methanesulfonyl group (**Xa**) were effective for stabilization of VDR. From the docking model (Fig. 3(d)), it appears that a hydrogen-bonding interaction between the sulfonyl group in **Xa** and Arg274 contributes to the stabilization.

Based upon these docking calculations, we selected **IIb**, **IId–e**, **IIIa–c**, **IVd**, **Va–d**, **VIIe**, **VIIIa**, and **Xa** as synthetic targets.

2. Synthesis of 2-*N*-substituted vitamin D derivatives

Palladium-catalyzed coupling reaction of vinyl bromide **5** (CD-ring) with an ene–yne-type A-ring synthon was developed by Trost for the synthesis of 2-*N*-substituted vitamin D derivatives.[17] We planned to synthesize A-ring precursors of 2α- and 2β-*N*-substituted ene–ynes **6** and **7** from L-serine (**8**) as a single chiral source by switching the positions of the vinyl and propargyl groups, as depicted in Scheme 1.

A-ring synthons for 2α-*N*-substituted-1,25-VD_3 derivatives **14–24** were synthesized from the key amine intermediate **13** (Scheme 2). Optically active allyl alcohol **9** was obtained from L-serine (**8**) according to Katsumura's method.[18] The hydroxyl group of **9** was protected with TBS ether to give bis-TBS ether **10** in 93% yield. The primary TBS group in **10** was selectively deprotected with 1% HCl in ethanol to give alcohol **11**. In this reaction, the diol was co-generated in 23% yield, with 16% recovery of the starting bis-TBS ether **10**. The diol was quantitatively transformed back to the starting bis-TBS ether **10** with TBSOTf and 2,6-lutidine. Oxidation of the hydroxyl group under Swern conditions followed by reaction with propargyl Grignard reagent gave the alcohol as a 1 : 1 mixture of diastereomers,[19] which were separated by column chromatography on silica gel to give **12** in 53% yield from **11**. The TBS ether and Boc group in **12** were deprotected with TFA, and resulting diol was protected as TBS ether with TBSOTf and 2,6-lutidine to afford the key amine intermediate **13** in 75% yield. *N*,*N*′-Dialkyl A-ring synthons **14–16** were synthesized in 51–60% yields by reductive amination with the corresponding aldehydes. In the case of NBn_2-substituted **16**, *N*-alkylation of amine **13** with benzyl bromide in the presence of potassium carbonate was more effective than a reductive amination protocol. *N*-Acyl derivatives **17–19** were synthesized by reaction with acyl halide or acyl anhydride in 90–96% yields. *N*-Sulfonamide derivatives **20–23** were synthesized by reaction of sulfonyl chloride in the

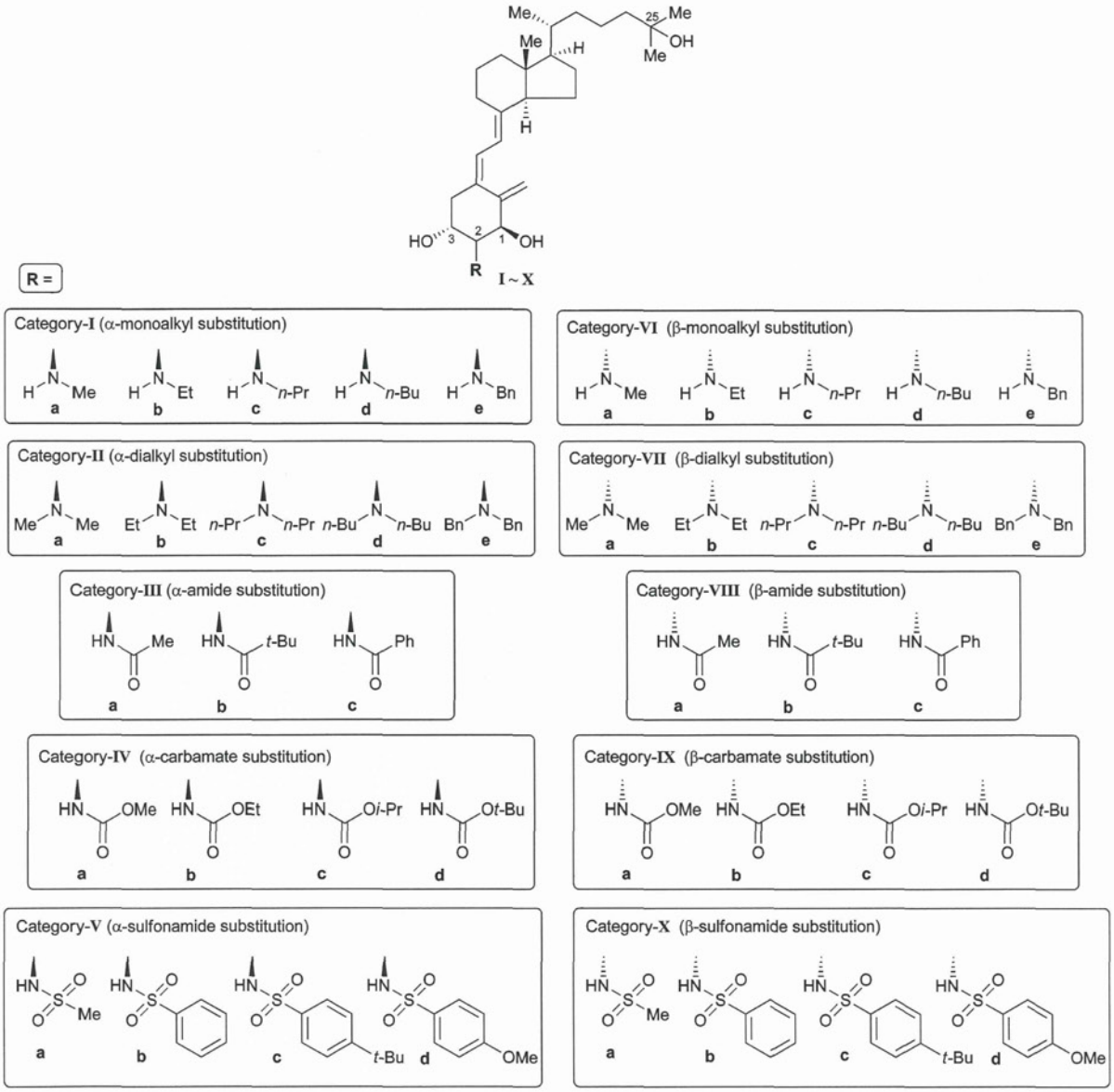

Fig. 2 Structures of 2-*N*-substituted vitamin D_3 derivatives.

Table 1 Docking scores of 2-*N*-substituted vitamin D_3 derivatives with the AF2 domain of VDR calculated with Glide XP

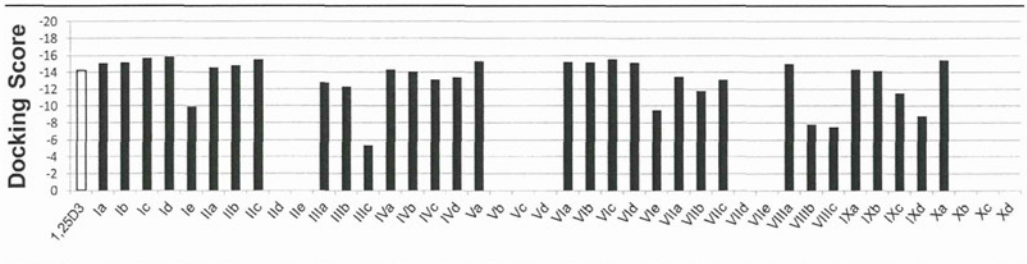

presence of triethylamine in 80–95% yields. The *N*-carbamate derivative **24** was synthesized from **12** by silylation with TBSOTf and 2,6-lutidine in 38% yield.

Other A-ring synthons with 2β stereochemistry **32–34** were also synthesized from L-serine (**8**) (Scheme 3). Optically active Weinreb amide **25**,[20] derived from L-serine (**8**), was reacted with

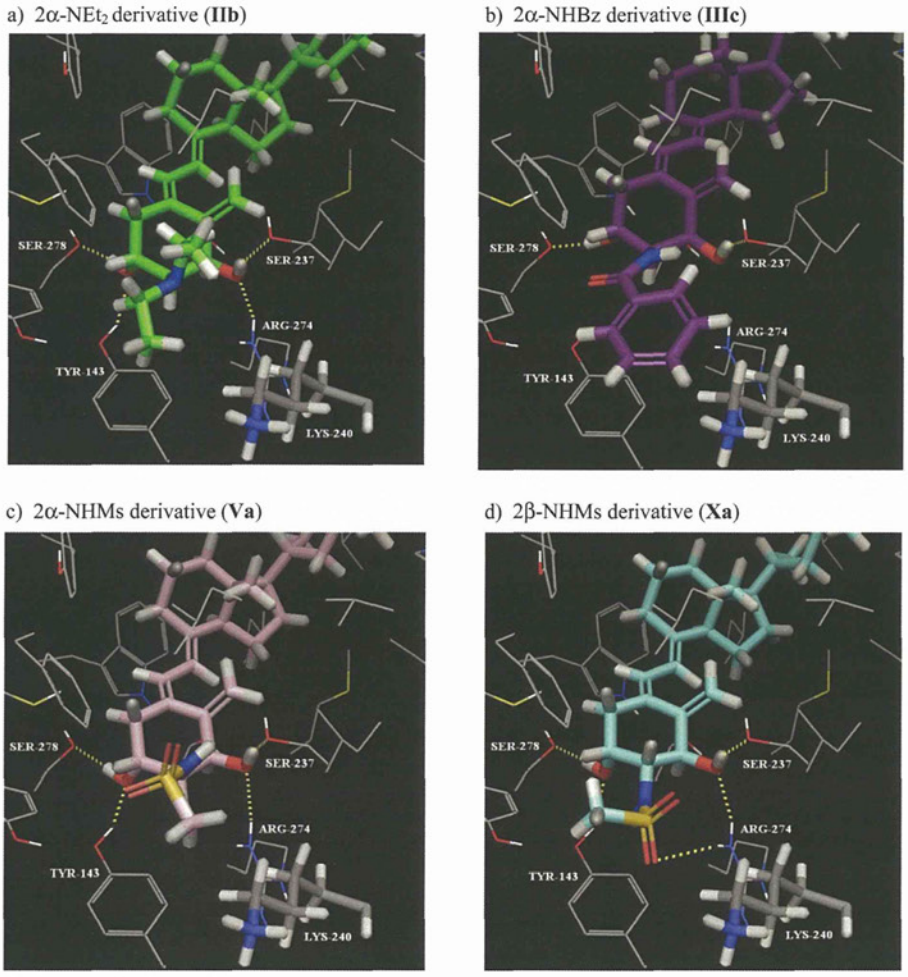

Fig. 3 Selected docking models of 2-*N*-substituted 1,25-VD_3 with the AF2 domain of VDR calculated with Autodock.

vinyl magnesium bromide to give vinyl ketone **26** in 85% yield. Reduction of the ketone with zinc borohydride proceeded stereoselectively, affording the alcohol as a single stereoisomer,[21] whose hydroxyl group was protected as TBS ether to give **27** in 89% yield in 2 steps. Ozonolysis of the vinyl group of **27** followed by reduction of the resulting ozonide with sodium borohydride gave the alcohol, which was treated with methanesulfonyl chloride followed by TBAF to give epoxide **28** in 76% yield in 3 steps.[22] Opening reaction of the epoxide was carried out with trimethylsilyl acetylide in the presence of $BF_3{\cdot}Et_2O$, and the resulting hydroxyl group was protected with *tert*-butyldiphenyl chloride (TBDPSCl) to give TBDPS ether **29** in 87% yield. The acetonide in **29** was deprotected with bismuth tribromide,[24] and the alcohol was oxidized with TPAP to give the aldehyde, which was subsequently reacted with vinylmagnesium bromide to give alcohol **30** as a mixture of two diastereomers (dr = 1 : 1) in 59% yield in 3 steps. After separation of the diastereomers on a silica gel column, deprotection of the TBDPS and TMS groups and the Boc group was conducted with TBAF and TFA, respectively, to give the diol, whose hydroxyl groups were protected as TBS ethers to give amine **31** in 61% yield. This key intermediate was converted into *N*,*N*′-dibenzyl **32**, *N*-acetyl **33** and *N*-methanesulfonyl **34** by following the same procedures described for the synthesis of the corresponding 2α-stereoisomers of A-ring synthons **16**, **17**, and **20**.

With the *N*-substituted A-ring synthons with 2α and 2β stereochemistry, **14–24** and **32–34**, in hand, these A-ring precursors were coupled with the CD-ring bromomethylene **5** in the presence of $Pd(PPh_3)_4$,[17] and the resulting TBS-protected coupling products were deprotected with TBAF or HF–Et_3N (Scheme 4) to afford the 2α-*N*-substituted vitamin D_3 derivatives **II–V**. 2β-*N*-Substituted 1,25-VD_3 derivatives **VIIe**, **VIIIa** and **Xa** were also obtained in 33, 17 and 21% yields, respectively.[25]

3. Evaluation of VDR-mediated transcription-activating activity of 2-*N*-substituted 1,25-VD_3 derivatives

The biological activities of these 2-*N*-substituted 1,25-VD_3 derivatives were evaluated by means of a luciferase-based VDR transcriptional activity assay in NIH3T3 cells.[26] NIH3T3 cells

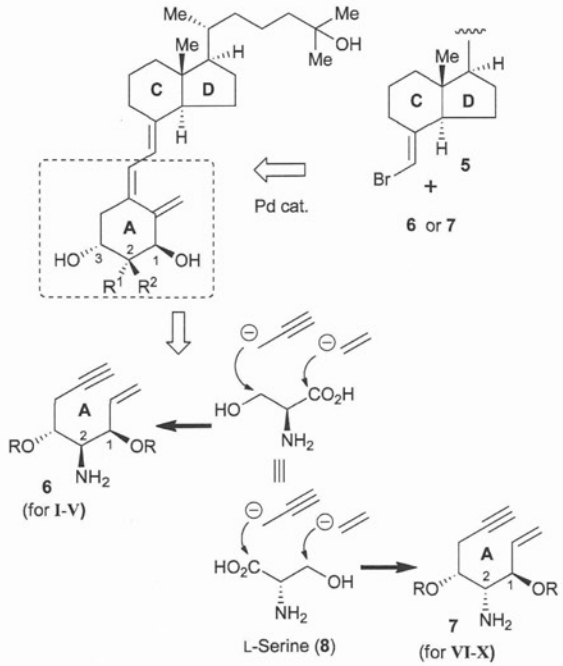

Scheme 1 Synthetic plan for A-ring synthons **6** and **7** of 2-*N*-substituted vitamin D_3 derivatives.

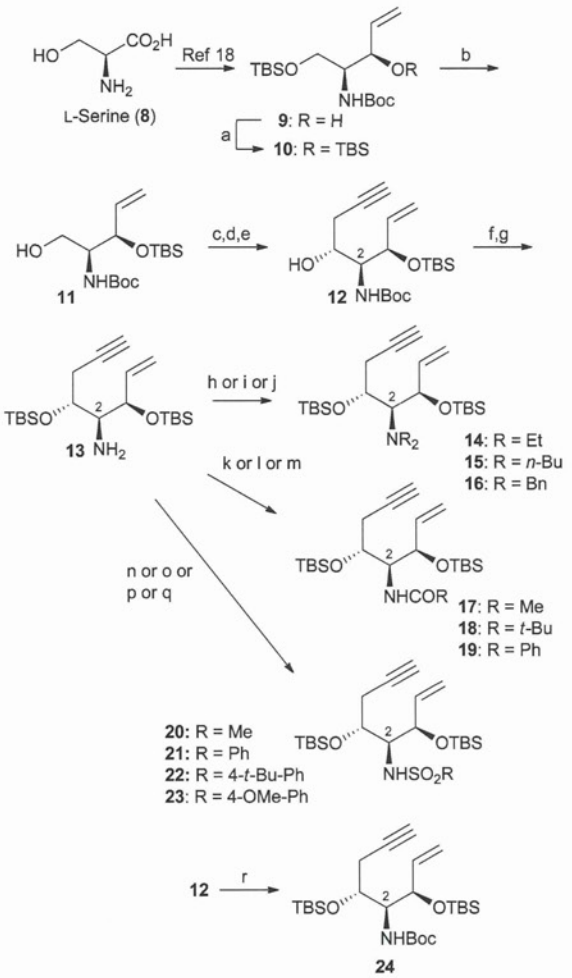

Scheme 2 Synthesis of 2α-*N*-substituted A-ring synthons **14–24**. (a) TBSCl, imidazole, DMAP, DMF, rt, 93%; (b) 1% HCl, EtOH, rt, 60% (diol was generated in 23% yield, with 16% recovery of starting bis-TBS ether **10**); (c) $(COCl)_2$, DMSO, *i*-Pr_2NEt, CH_2Cl_2, −78 °C to 0 °C; (d) propargyl magnesium bromide, THF, 0 °C; (e) Separation with silica gel column, 53% (C3 isomer 35%); (f) 20% TFA–CH_2Cl_2, 0 °C to rt; (g) TBSOTf, 2,6-lutidine, CH_2Cl_2, 0 °C to rt, 75% (2 steps); (h) acetoaldehyde (6 eq), $NaBH_3CN$, then AcOH, CH_3CN, 0 °C to rt, 51%; (i) *n*-butylaldehyde (6 eq), $NaBH_3CN$, then AcOH, CH_3CN, 0 °C to rt, 59%; (j) BnBr, K_2CO_3, CH_3CN, 80 °C, 60%; (k) acetic anhydride, rt, 94%; (l) pivaloyl chloride, triethylamine, CH_2Cl_2, 0 °C to rt, 96%; (m) benzoic anhydride, triethylamine, THF, 0 °C to rt, 90%; (n) methanesulfonyl chloride, triethylamine, CH_2Cl_2, 0 °C to rt, 95%; (o) benzenesulfonyl chloride, triethylamine, CH_2Cl_2, rt, 83%; (p) 4-*t*-butylbenzenesulfonyl chloride, triethylamine, THF, rt, 80%; (q) 4-methoxybenzenesulfonyl chloride, triethylamine, THF, rt, 93%; (r) TBSOTf, 2,6-lutidine, CH_2Cl_2, 0 °C, 38%.

were transfected with pDR3-Luc and pGL4.74 [hLuc/TK] normalizing vectors, then treated with 1,25-VD_3 or compounds (100 nM **IIb**, **IId–e**, **IIIa–c**, **IVd**, **Va–d**, **VIIe**, **VIIIa**, and **Xa**), and the luciferase activity was measured. The relative intensities of the luciferase activity of compounds *versus* the control or 1,25-VD_3 are summarized in Fig. 4.

Among the compounds tested, 2α-NHAc-1,25-VD_3 (**IIIa**) showed similar activity to 1,25-VD_3, while **IVd** and **Va**, bearing NHBoc and NHMs groups at 2α, showed moderate activity. Among the 2β stereoisomers, the 2β-*N*-acetyl derivative (**VIIIa**), which effectively stabilized VDR in the docking studies, showed potent activity nearly equal to that of 1,25-VD_3. However, 2β-NHMs-1,25-VD_3 (**Xa**), which appeared to exhibit a hydrogen-bonding interaction with Arg274 of VDR in the docking studies, showed the highest transcriptional activity among the derivatives synthesized, being slightly more potent than VD_3. These derivatives all have a hydrogen-bond-donating group at the C2 position, so hydrogen bonding seems to be important for VDR transcriptional activity. Indeed, 2α-NEt_2-1,25-VD_3 (**IIb**), which cannot form a hydrogen bond, induced no transcriptional activity, although it could be well docked with VDR by calculation. Steric hindrance is also an important factor. Compounds **IIe** and **VIIe** bearing bulky *N*,*N*′-Bn_2 groups at the 2α- and 2β-position, respectively, gave no calculated docking poses with VDR, and also failed to induce transcriptional activity. On the other hand, $NHSO_2Ar$ can act as a hydrogen bond donor, but it is a bulky group, and it induced only low transcriptional activity. Thus, it appears that 2-*N*-substituted 1,25-VD_3 derivatives with a relatively small substituent group that has hydrogen-bond donor capability are effective for eliciting VDR transcriptional activity.

4. Conclusion

In summary, we carried out computational docking with VDR for a series of novel 2α- and 2β-*N*-substituted 1,25-VD_3 derivatives. Based on the results, 14 compounds were selected and synthesized. A-Ring synthons for both stereoisomers were synthesized from L-serine (**8**) as a single chiral source by installing vinyl and propargyl groups at opposite ends of the molecule.

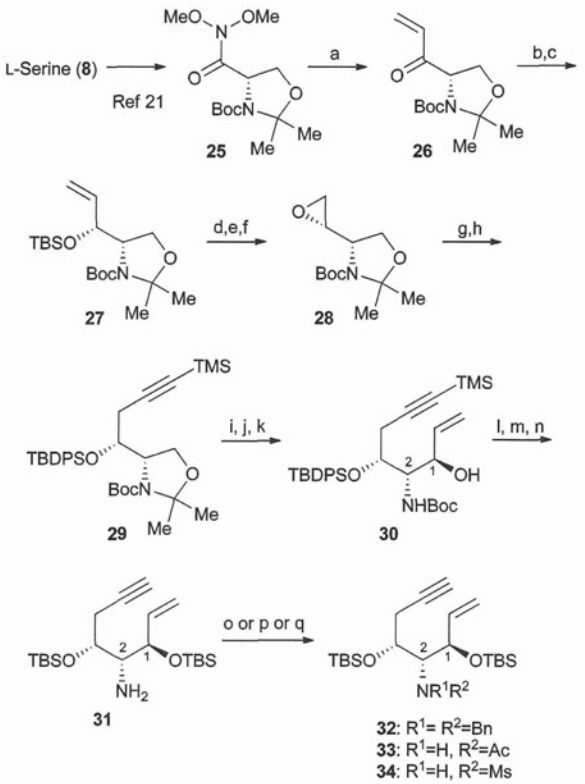

Scheme 3 Synthesis of 2β-substituted A-ring synthons **32–34**. (a) vinyl magnesium bromide, THF, 0 °C, 85%; (b) $Zn(BH_4)_2$, Et_2O, −30 °C; (c) TBSCl, imidazole, DMAP, DMF, rt, 89% (2 steps); (d) O_3, CH_2Cl_2, MeOH, −78 °C, then $NaBH_4$, −78 °C to rt; (e) MsCl, triethylamine, CH_2Cl_2, 0 °C, 94% (2 steps); (f) TBAF, THF, rt, 81%; (g) trimethylsilyl acetylene, *n*-BuLi, $BF_3{\cdot}Et_2O$, THF, −78 °C, 90%; (h) TBDPSCl, imidazole, DMF, rt to 40 °C, 97%; (i) $BiBr_3$, CH_3CN–H_2O, rt, 91%; (j) TPAP, NMO, MS-4A, CH_2Cl_2, rt, 92%; (k) vinyl magnesium bromide, THF, 0 °C, then separation (α-isomer: 35%, β-isomer: 35%); (l) TBAF, THF, rt, 89%; (m) 20% TFA–CH_2Cl_2, 0 °C to rt; (n) TBSOTf, 2,6-lutidine, CH_2Cl_2, 0 °C to rt, 69% (2 steps); (o) BnBr, K_2CO_3, CH_3CN, NaI, 80 °C, 54%; (p) Ac_2O, rt, 99%; (q) MsCl, Et_3N, CH_2Cl_2, 0 °C to rt, 84%.

These A-rings were coupled with CD-ring bromomethylene **5** according to Trost's protocol to afford the target compounds. In a dual-luciferase reporter assay, **IIIa**, **VIIIa** and **Xa** showed similar activity to 1,25-VD_3. Our results indicate that 2-*N*-substituted 1,25-VD_3 derivatives with a relatively small substituent group that has the potential to form a hydrogen bond with the receptor are effective for eliciting VDR transcriptional activity. Further structural development studies and evaluation of various VDR-mediated biological activities of our compounds are in progress.

Experimental

General

Flash chromatography was performed on Silica gel 60 (spherical, particle size 40–100 μm; Kanto). Optical rotations were measured on a JASCO P-2200 polarimeter. ^1H and ^{13}C NMR

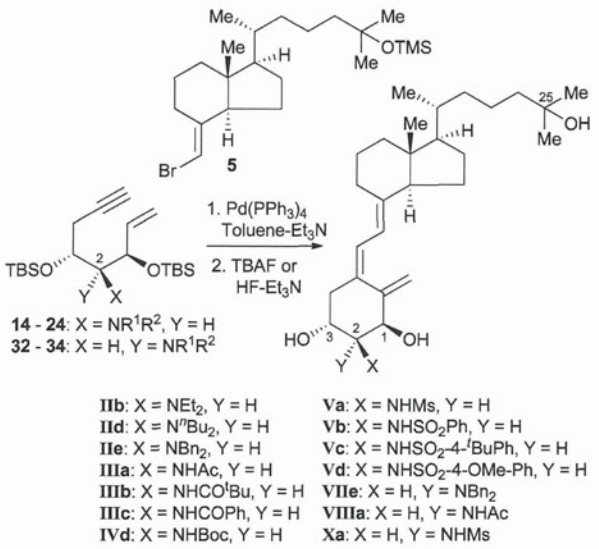

Scheme 4 Synthesis of 2α-*N*-substituted 1,25-VD_3 derivatives; **IIb** (NEt_2), 20%; **IId** (N-nBu_2), 10%; **IIe** (NBn_2), 10%; **IIIa** (NHAc), 9%; **IIIb** (NHCO-*t*Bu), 57%; **IIIc** (NHCOPh), 25%; **IVd** (NHBoc), 20%; **Va** ($NHSO_2Me$), 57%; **Vb** ($NHSO_2Ph$), 5%; **Vc** ($NHSO_2$-4-*t*BuPh), 8%; **Vd** ($NHSO_2$-4-OMe-Ph), 6%. Synthesis of 2β-*N*-substituted 1,25-VD_3 derivatives; **VIIe** (NBn_2), 33%; VIIIa (NHAc), 17%; **Xa** ($NHSO_2Me$), 21%.

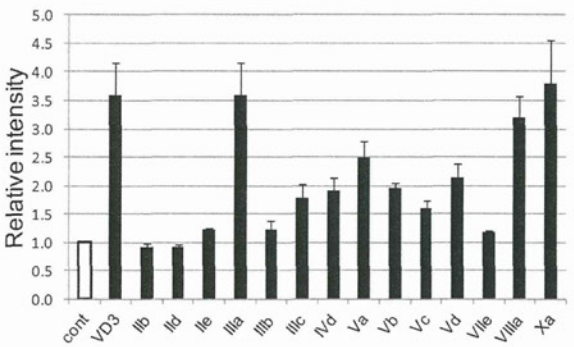

Fig. 4 Results of dual-luciferase reporter assay for 2-*N*-substituted 1,25-VD_3 derivatives. Data are expressed as the means ± SEM.

spectra were recorded on JEOL JNM-ECA 500, JNM-ECX 400 or JMTC 300. The spectra are referenced internally according to residual solvent signals of $CDCl_3$ (^1H NMR; δ = 7.26 ppm, ^{13}C NMR; δ = 77.0 ppm). Data for ^1H NMR are recorded as follows: chemical shift (δ, ppm), multiplicity (s, singlet; d, doublet; t, triplet; q, quartet; m, multiplet; br, broad), integration, coupling constant (Hz). Data for ^{13}C NMR are reported in terms of chemical shift (δ, ppm). Mass spectra were recorded on JEOL JMS-T100X spectrometer with ESI-MS mode using methanol as solvent.

Bis-TBS ether 10. To a solution of **9** (16.7 mmol) in DMF (50 mL) was added imidazole (2.7 g, 40.1 mmol), DMAP (204 mg, 1.67 mmol) and TBSCl (3 g, 20.0 mmol), and the mixture was stirred for 24 h at room temperature. To the reaction mixture was added H_2O and then it was extracted with ethyl

acetate. The organic layer was washed with H_2O and brine, and the extracts were dried over $MgSO_4$, filtered, and concentrated *in vacuo*. The residue was purified by silica gel chromatography (hexane–ethyl acetate = 100 : 1) to give **10** (6.9 g, 15.5 mmol, 93%). $[\alpha]_D^{22}$ = +3.4 (*c* 1.3, $CHCl_3$); ^{1}H NMR (400 MHz, $CDCl_3$) δ 5.76–5.90 (m, 1H), 5.10–5.28 (m, 2H), 4.62 (d, *J* = 7.3 Hz, 1H), 4.27 (brs, 1H), 3.76 (m, 1H), 3.69–3.55 (m, 2H), 1.42 (s, 9H), 0.89 (s, 9H), 0.88 (s, 9H), 0.07–0.01 (m, 12H); ^{13}C NMR (75 MHz, $CDCl_3$) δ 155.6, 138.3, 116.2, 79.0, 73.1, 61.3, 56.4, 28.4, 25.8, 18.2, 18.1, −5.3, −5.5; HRMS: calcd for $C_{22}H_{47}NO_4Si_2Na$, 468.2941; found, 468.2940.

Alcohol 11. A solution of **10** (3.2 g, 7.18 mmol) in HCl and ethanol (1 : 99, 240 mL) was stirred for 15 min at room temperature. To the reaction mixture was added saturated $NaHCO_3$, then it was concentrated *in vacuo*. The residue was extracted with ethyl acetate and the organic layer was washed with H_2O and brine, and dried over $MgSO_4$, filtered, and concentrated *in vacuo*. The residue was purified by silica gel chromatography (hexane–ethyl acetate = 4 : 1) to give **11** (1.43 g, 4.31 mmol, 60%). $[\alpha]_D^{22}$ = −20.8 (*c* 5.2, $CHCl_3$); ^{1}H NMR (500 MHz, $CDCl_3$) δ 5.88–5.79 (m, 1H), 5.40–5.18 (m, 3H), 4.52 (s, 1H), 3.97 (d, *J* = 11.4 Hz, 1H), 3.60–3.45 (m, 2H), 1.43 (s, 9H), 0.91–0.86 (m, 9H), 0.08–0.02 (m, 6H); ^{13}C NMR (125 MHz, $CDCl_3$) δ 155.7, 137.5, 116.3, 79.5, 76.0, 61.9, 54.6, 28.3, 25.7, 25.6, 18.0, −3.6; HRMS: calcd for $C_{16}H_{33}NO_4SiNa$, 354.2077; found, 354.2060.

Alcohol 12. To a solution of $(COCl)_2$ (0.6 mL, 7.29 mmol) in dichloromethane (30 mL) was added DMSO (1 mL, 14.3 mmol) dropwise at −78 °C. The reaction mixture was stirred for 10 min at −78 °C, and to the mixture was added dropwise a solution of **11** (1.05 g, 3.17 mmol) in dichloromethane (20 mL). The reaction mixture was stirred for 1.5 h at −78 °C, and diisopropylethylamine (5 mL, 28.5 mmol) was added. The resulting mixture was warmed to room temperature for 30 min. To the reaction mixture was added 1 N HCl, and the mixture was extracted with dichloromethane. The extracts were washed with H_2O, dried over $MgSO_4$, filtered, and concentrated *in vacuo* to give aldehyde. To a prepared solution of propargyl magnesium bromide (1 M in THF, 17 mL, 17.1 mmol) was added aldehyde in THF (15 mL) at 0 °C, and the mixture was stirred for 40 min. The resulting mixture was quenched by 1 N HCl at 0 °C and extracted with ethyl acetate. The organic layer was washed with H_2O and brine, and the extracts were dried over $MgSO_4$, filtered, and concentrated *in vacuo*. The residue was purified by silica gel chromatography (hexane–ethyl acetate = 13 : 1) to give **12** (148 mg, 0.296 mmol, 53% from **11**). $[\alpha]_D^{22}$ = −25.6 (*c* 2.2, $CHCl_3$); ^{1}H NMR (500 MHz, $CDCl_3$) δ 5.90–5.82 (m, 1H), 5.39–5.20 (m, 3H), 4.61–4.57 (m, 1H), 4.27 (t, *J* = 6.9 Hz, 1H), 3.61 (s, 1H), 3.58 (dd, *J* = 8.9, 2.0 Hz, 1H), 2.35 (ddd, *J* = 58.3, 16.5, 2.9 Hz, 2H), 2.01 (t, *J* = 2.9 Hz, 1H), 1.44 (s, 9H), 0.91 (s, 9H), 0.08 (s, 3H), 0.04 (s, 3H); ^{13}C NMR (125 MHz, $CDCl_3$) δ 155.6, 137.2, 116.7, 80.5, 79.6, 76.6, 70.1, 68.3, 55.0, 28.4, 25.8, 23.6, 18.0, −4.8, −5.3; HRMS: calcd for $C_{19}H_{35}NO_4SiNa$, 392.2233; found, 392.2267.

Amine 13. A solution of **12** (298 mg, 0.81 mmol) in TFA and dichloromethane (1 : 4, 8 mL) was stirred at 0 °C for 5 min and room temperature for 1 h. The reaction mixture was concentrated *in vacuo* to give diol. To a solution of the resulting diol in dichloromethane (8 mL) was added 2,6-lutidine (0.6 mL, 4.84 mmol) and TBSOTf (0.6 mL, 2.42 mmol), and the mixture was stirred at 0 °C for 40 min. To the reaction mixture was added saturated $NaHCO_3$, then it was extracted with ethyl acetate. The organic layer was washed with H_2O and brine, and dried over $MgSO_4$, filtered, and concentrated *in vacuo*. The residue was purified by silica gel chromatography (hexane–ethyl acetate = 40 : 1) to give **13** (250 mg, 0.65 mmol, 75% from **12**). $[\alpha]_D^{24}$ = −3.6 (*c* 0.2, $CHCl_3$); ^{1}H NMR (400 MHz, $CDCl_3$) δ 5.83–5.74 (m, 1H), 5.26–5.17 (m, 2H), 4.10–4.04 (m, 1H), 3.95 (t, *J* = 7.4 Hz), 2.86 (dd, *J* = 6.9, 2.8 Hz, 1H), 2.65–2.32 (m, 2H), 1.99 (t, *J* = 2.7 Hz, 1H), 0.91–0.88 (m, 18H), 0.12–0.03 (m, 12H); ^{13}C NMR (100 MHz, $CDCl_3$) δ 139.2, 117.8, 81.2, 76.4, 70.4, 70.2, 58.3, 25.9, 24.9, 18.1, −3.3, −4.0; HRMS: calcd for $C_{20}H_{42}NO_2Si_2$, 384.2754; found, 384.2725.

2α-*N*-Ethylamine 14. To a solution of **13** (100 mg, 0.26 mmol) in acetonitrile (2.6 mL) was added acetoaldehyde (88 μL, 1.56 mmol) and $NaBH_3CN$ (41 mg, 0.65 mmol) at room temperature, and the mixture was stirred for 50 min. To the reaction mixture was added acetic acid until the pH of the mixture reached 3. The resulting mixture was stirred for 1.5 h and quenched by saturated $NaHCO_3$. The reaction mixture was extracted with ethyl acetate. The organic layer was washed with brine, and the extracts were dried over $MgSO_4$, filtered, and concentrated *in vacuo*. The residue was purified by silica gel chromatography (hexane–ethyl acetate = 100 : 1) to give **14** (58 mg, 0.13 mmol, 51%). $[\alpha]_D^{20}$ = +4.8 (*c* 0.9, $CHCl_3$); ^{1}H NMR (400 MHz, $CDCl_3$) δ 5.98–5.87 (m, 1H), 5.28–5.12 (m, 2H), 4.38 (t, *J* = 8.9 Hz, 1H), 4.28–422 (m, 1H), 2.88–2.74 (m, 4H), 2.65–2.57 (m, 2H), 2.28–2.20 (m, 1H), 1.95 (t, *J* = 2.8 Hz, 1H), 0.97 (t, *J* = 7.1 Hz, 6H), 0.9–0.86 (m, 18H), 0.13–0.02 (m, 12H); ^{13}C NMR (100 MHz, $CDCl_3$) δ 141.9, 117.2, 82.4, 74.3, 72.3, 69.8, 67.0, 47.9, 26.0, 24.4, 18.1, 16.4, −2.4, −4.1, −4.6; HRMS: calcd for $C_{24}H_{50}NO_2Si_2$, 440.3380; found, 440.3353.

2α-*N*-*n*-Butylamine 15. To a solution of **13** (100 mg, 0.26 mmol) in acetonitrile (2.6 mL) was added *n*-butylaldehyde (140 μL, 1.56 mmol) and $NaBH_3CN$ (41 mg, 0.65 mmol) at room temperature, and the mixture was stirred for 1 h. To the reaction mixture was added acetic acid until the pH of the mixture reached 3. The resulting mixture was stirred for 1 h and quenched by saturated $NaHCO_3$. The reaction mixture was extracted with ethyl acetate. The organic layer was washed with brine, and the extracts were dried over $MgSO_4$, filtered, and concentrated *in vacuo*. The residue was purified by silica gel chromatography (hexane–ethyl acetate = 100 : 1) to give **15** (76 mg, 0.15 mmol, 59%). $[\alpha]_D^{21}$ = +1.6 (*c* 0.6, $CHCl_3$); ^{1}H NMR (400 MHz, $CDCl_3$) δ 6.03–5.88 (m, 1H), 5.30–5.12 (m, 2H), 4.40 (t, *J* = 8.6 Hz, 1H), 4.28–4.20 (m, 1H), 2.89–2.62 (m, 5H), 2.60–2.49 (m, 2H), 2.31–2.21 (m, 1H), 1.95 (t, *J* = 2.5 Hz, 1H), 1.42–1.30 (m, 4H), 1.29–1.14 (m, 4H), 0.84–0.92 (m, 24H), 0.15–0.02 (m, 12H); ^{13}C NMR (75 MHz, $CDCl_3$) δ 141.9, 117.1, 82.5, 74.6, 72.5, 69.9, 67.6, 54.6, 33.3, 26.0, 24.6, 20.5, 18.1, −2.4, −4.1; HRMS: calcd for $C_{28}H_{58}NO_2Si_2$, 496.4006; found, 496.4010.

2α-*N*,*N*′-Dibenzylamine 16. To a solution of **13** (100 mg, 0.26 mmol) in acetonitrile (3 mL) was added K_2CO_3 (360 mg,

2.61 mmol) and BnBr (0.13 mL, 2.61 mmol) at room temperature, and the mixture was stirred at 80 °C for 10 h. To the resulting mixture was added saturated NH_4Cl, and the mixture was extracted with ethyl acetate. The organic layer was washed with brine, and the extracts were dried over $MgSO_4$, filtered, and concentrated *in vacuo*. The residue was purified by silica gel chromatography (hexane–ethyl acetate = 100 : 1) to give **16** (89 mg, 0.16 mmol, 60%). $[\alpha]_D^{24}$ = −14.4 (*c* 3.9, $CHCl_3$); ^{1}H NMR (400 MHz, $CDCl_3$) δ 7.40–7.16 (m, 10H), 6.08–5.97 (m, 1H), 5.44–5.27 (m, 2H), 4.54 (t, *J* = 8.7 Hz, 1H), 4.s35–4.29 (m, 1H), 3.96 (dd, *J* = 134.7, 13.8 Hz, 4H), 2.91 (dd, *J* = 8.5, 2.6 Hz, 1H), 2.67–2.58 (m, 1H), 2.39–2.31 (m, 1H), 1.68 (t, *J* = 2.5 Hz, 1H), 0.89 (s, 9H), 0.82 (s, 9H), 0.13–0.03 (m, 12H); ^{13}C NMR (100 MHz, $CDCl_3$) δ 142.0, 140.9, 129.4, 127.9, 126.5, 117.6, 81.6, 75.1, 72.8, 69.8, 63.8, 56.5, 25.9, 18.1, −2.5, −4.0, −4.5; HRMS: calcd for $C_{34}H_{54}NO_2Si_2$, 564.3693; found, 564.3682.

2α-*N*-Acetylamine 17. A solution of **13** (66 mg, 0.17 mmol) in acetic anhydride (0.5 mL) was stirred for 15 min at room temperature. The resulting mixture was concentrated *in vacuo* to give **17** (69 mg, 0.16 mmol, 94%). $[\alpha]_D^{25}$ = −12.8 (*c* 0.4, $CHCl_3$); ^{1}H NMR (500 MHz, $CDCl_3$) δ 5.91–5.82 (m, 1H), 5.69 (d, *J* = 9.7 Hz, 1H), 5.15–5.03 (m, 2H), 4.32–4.27 (m, 1H), 4.11 (t, *J* = 9.2 Hz, 1H), 3.96 (t, *J* = 8.6 Hz, 1H), 2.40–2.26 (m, 2H), 2.02 (t, J = 2.6 Hz, 1H), 1.94 (s, 3H), 0.92 (s, 9H), 0.88 (s, 9H), 0.14 (d, *J* = 4.0 Hz, 6H), 0.05 (s, 6H); ^{13}C NMR (125 MHz, $CDCl_3$) δ 169.8, 139.4, 117.4, 75.9, 70.9, 68.7, 55.8, 25.9, 25.4, 23.6, 18.1, −2.9, −4.0, −4.6; HRMS: calcd for $C_{22}H_{43}NO_3Si_2Na$, 448.2679; found 448.2674.

2α-*N*-Pivaloylamine 18. To a solution of **13** (60 mg, 0.16 mmol) in dichloromethane (1.6 mL) was added Et_3N (33 μL, 0.23 mmol) and pivaloyl chloride (23 μL, 0.19 mmol) at room temperature, and the mixture was stirred for 4 h. To the reaction mixture was added saturated NH_4Cl, and the mixture was extracted with ethyl acetate. The organic layer was washed with brine, and the extracts were dried over $MgSO_4$, filtered, and concentrated *in vacuo*. The residue was purified by silica gel chromatography (hexane–ethyl acetate = 20 : 1) to give **18** (71 mg, 0.15 mmol, 96%). $[\alpha]_D^{27}$ = −1.6 (*c* 1.1, $CHCl_3$); ^{1}H NMR (400 MHz, $CDCl_3$) δ 6.03 (d, *J* = 9.1 Hz, 1H), 5.91–5.80 (m, 1H), 5.11–5.01 (m, 2H), 4.34–4.29 (m, 1H), 4.06 (t, *J* = 9.2 Hz, 1H), 3.93 (t, *J* = 8.7 Hz, 1H), 2.31–2.24 (m, 2H), 2.00 (t, *J* = 2.8 Hz, 1H), 1.14 (s, 9H), 0.92 (s, 9H), 0.88 (s, 9H), 0.14 (s, 6H), 0.05 (s, 6H); ^{13}C NMR (100 MHz, $CDCl_3$) δ 177.7, 139.5, 117.2, 80.4, 76.2, 70.9, 69.1, 55.1, 38.7, 27.6, 25.9, 25.4, 18.0, −2.9, −4.0, −4.5, −4.6; HRMS: calcd for $C_{25}H_{49}NO_3Si_2Na$, 490.3149; found, 490.3123.

2α-*N*-Benzoylamine 19. To a solution of **13** (120 mg, 0.31 mmol) in THF (3 mL) was added triethylamine (90 μL, 0.63 mmol) and benzoic anhydride (106 mg, 0.47 mmol) at room temperature, and the mixture was stirred for 15 min. To the resulting mixture was added saturated NH_4Cl, and the mixture was extracted with ethyl acetate. The organic layer was washed with brine, and the extracts were dried over $MgSO_4$, filtered, and concentrated *in vacuo*. The residue was purified by silica gel chromatography (hexane–ethyl acetate = 20 : 1) to give **19** (136 mg, 0.28 mmol, 90%). $[\alpha]_D^{25}$ = −17.2 (*c* 1.2, $CHCl_3$); ^{1}H NMR (400 MHz, $CDCl_3$) δ 7.74–7.68 (m, 2H), 7.50–7.38 (m, 3H), 6.54 (d, *J* = 9.7 Hz, 1H), 6.01–5.91 (m, 1H), 5.14–5.06 (m, 2H), 4.42–4.38 (m, 1H), 4.34 (t, *J* = 9.2 Hz, 1H), 4.09 (t, *J* = 8.7 Hz, 1H), 2.47–2.30 (m, 2H), 2.00 (t, *J* = 2.7 Hz, 1H), 0.95 (s, 9H), 0.90 (s, 9H), 0.17 (d, *J* = 5.5 Hz, 6H), 0.68 (d, *J* = 1.8 Hz, 6H); ^{13}C NMR (100 MHz, $CDCl_3$) δ 166.9, 139.3, 135.0, 131.3, 128.6, 126.7, 117.7, 80.2, 76.1, 71.0, 69.1, 56.1, 25.9, 25.6, 18.1, −2.9, −4.0, −4.6; HRMS: calcd for $C_{27}H_{45}NO_3Si_2Na$, 510.2836; found, 510.2806.

2α-*N*-Methanesulfonylamine 20. To a solution of **13** (60 mg, 0.16 mmol) in dichloromethane (2 mL) was added triethylamine (53 μL, 0.37 mmol) and methanesulfonyl chloride (15 μL, 0.19 mmol) at 0 °C, and the mixture was stirred for 40 min at room temperature. To the resulting mixture was added saturated $NaHCO_3$, and the mixture was extracted with ethyl acetate. The organic layer was washed with brine, and the extracts were dried over $MgSO_4$, filtered, and concentrated *in vacuo*. The residue was purified by silica gel chromatography (hexane–ethyl acetate = 20 : 1) to give **20** (69 mg, 0.19 mmol, 95%). $[\alpha]_D^{26}$ = −5.0 (*c* 0.9, $CHCl_3$); ^{1}H NMR (400 MHz, $CDCl_3$) δ 5.94–5.84 (m, 1H), 5.32–5.23 (m, 2H), 4.65 (d, *J* = 9.2 Hz, 1H), 4.23–4.17 (m, 1H), 4.11 (t, *J* = 6.9 Hz, 1H), 3.77–3.70 (m, 1H), 3.03 (s, 3H), 2.58–2.48 (m, 1H), 2.41–2.33 (m, 1H), 2.07 (t, *J* = 2.8 Hz, 1H), 0.89 (d, *J* = 1.8 Hz, 18H), 0.13 (d, *J* = 5.5 Hz, 6H), 0.08 (d, *J* = 5.0 Hz, 6H); ^{13}C NMR (100 MHz, $CDCl_3$) δ 138.5, 118.2, 79.9, 75.6, 71.5, 69.9, 60.5, 42.7, 25.8, 25.1, 18.2, 18.0, −3.5, −4.0, −4.6; HRMS: calcd for $C_{21}H_{43}NO_4SSi_2Na$, 484.2349; found, 484.2358.

2α-*N*-Benzenesulfonylamine 21. To a solution of **13** (110 mg, 0.29 mmol) in dichloromethane (3 mL) was added triethylamine (0.1 mL, 0.69 mmol) and benzenesulfonyl chloride (45 μL, 0.34 mmol) at room temperature, and the mixture was stirred for 6 h. The reaction mixture was diluted with H_2O and extracted with ethyl acetate. The organic layer was washed with brine, and the extracts were dried over $MgSO_4$, filtered, and concentrated *in vacuo*. The residue was purified by silica gel chromatography (hexane–ethyl acetate = 40 : 1) to give **21** (124 mg, 0.24 mmol, 83%). $[\alpha]_D^{18}$ = −26.5 (*c* 0.9, $CHCl_3$); ^{1}H NMR (400 MHz, $CDCl_3$) δ 7.91–7.85 (m, 2H), 7.59–7.44 (m, 3H), 5.74–5.62 (m, 1H), 5.13–4.85 (m, 2H), 4.15 (q, *J* = 4.6 Hz, 1H), 4.00 (t, *J* = 7.8 Hz, 1H), 3.58 (t, *J* = 8.3 Hz, 1H), 2.14–206 (m, 1H), 1.98 (t, *J* = 2.5 Hz, 1H), 1.93–1.83 (m, 1H), 0.86 (s, 18H), 0.07 (d, *J* = 5.5 Hz, 6H), 0.02 (d, *J* = 3.7 Hz, 6H); ^{13}C NMR (100 MHz, $CDCl_3$) δ 141.8, 138.7, 132.4, 128.9, 127.0, 118.1, 80.2, 75.7, 71.1, 69.4, 59.9, 24.8, 18.1, 18.0, −3.3, −4.3, −4.5, −4.7; HRMS: calcd for $C_{26}H_{45}NO_4SSi_2Na$, 546.2506; found, 546.2500.

2α-*N*-(4-*tert*-Butyl)-benzenesulfonylamine 22. To a solution of **13** (65 mg, 0.17 mmol) in THF (2 mL) was added triethylamine (57 μL, 0.41 mmol), 4-*tert*-butyl-benzenesulfonyl chloride (47 mg, 0.20 mmol) at room temperature, and the mixture was stirred for 8 h. The reaction mixture was warmed to 60 °C and stirred additional 8 h. The resulting mixture was diluted with H_2O at room temperature and the mixture was extracted with ethyl acetate. The organic layer was washed with brine, and the extracts were dried over $MgSO_4$, filtered, and concentrated *in vacuo*. The residue was purified by silica gel chromatography

(hexane–ethyl acetate = 30 : 1) to give **22** (78.9 mg, 0.14 mmol, 80%). $[\alpha]_D^{19}$ = −18.7 (*c* 2.7, $CHCl_3$); ^{1}H NMR (400 MHz, $CDCl_3$) δ 7.82–7.76 (m, 2H), 7.51–7.45 (m, 2H), 5.74–5.59 (m, 1H), 5.12–4.85 (m, 2H), 4.16–4.09 (m, 1H), 4.01 (t, *J* = 7.6 Hz, 1H), 3.58–3.48 (m, 1H), 2.16–1.92 (m, 3H), 1.33 (s, 9H), 0.86 (d, *J* = 1.4 Hz, 18H), 0.60 (s, 6H), 0.01 (d, *J* = 3.4 Hz, 6H); ^{13}C NMR (100 MHz, $CDCl_3$) δ 156.2, 138.7, 126.9, 125.8, 117.8, 80.4, 75.6, 70.9, 69.6, 59.9, 35.1, 31.1, 25.8, 24.8, 18.1, 18.0, −3.3, −4.3, −4.5, −4.7; HRMS: calcd for $C_{30}H_{53}NO_4SSi_2Na$, 602.3132; found, 602.3137.

2α-*N*-(4-Methoxy)-benzenesulfonylamine 23. To a solution of **13** (90 mg, 0.24 mmol) in THF (2 mL) was added triethylamine (79 μL, 0.56 mmol) and 4-methoxybenzenesulfonyl chloride (58 mg, 0.28 mmol) at room temperature, and the mixture was stirred for 3 h. To the reaction mixture was added saturated NH_4Cl, and the mixture was extracted with ethyl acetate. The organic layer was washed with brine, and the extracts were dried over $MgSO_4$, filtered, and concentrated *in vacuo*. The residue was purified by silica gel chromatography (hexane–ethyl acetate = 15 : 1) to give **23** (122 mg, 0.22 mmol, 93%). $[\alpha]_D^{18}$ = −27.2 (*c* 2.3, $CHCl_3$); ^{1}H NMR (400 MHz, $CDCl_3$) δ 7.80 (d, *J* = 9.0 Hz, 2H), 6.94 (d, *J* = 8.9 Hz, 2H), 5.77–5.62 (m, 1H), 5.14–5.03 (m, 2H), 4.84 (d, *J* = 8.9 Hz, 1H), 4.19–4.11 (m, 1H), 4.01 (t, *J* = 7.7 Hz, 1H), 3.86 (s, 3H), 3.58–3.49 (m, 1H), 2.18–1.89 (m, 3H), 0.86 (s, 18H), 0.07 (d, *J* = 2.4 Hz, 6H), 0.02 (d, *J* = 3.5 Hz, 6H); ^{13}C NMR (100 MHz, $CDCl_3$) δ 162.6, 138.8, 133.6, 129.2, 118.0, 114.0, 80.4, 75.7, 71.0, 69.4, 59.8, 55.6, 25.9, 24.9, 18.1, 18.0, −3.3, −4.3, −4.5, −4.7; HRMS: calcd for $C_{27}H_{47}NO_5SSi_2Na$, 576.2611; found, 576.2606.

2α-*N*-*tert*-Butoxycarbonylamine 24. To a solution of **12** (124 mg, 0.34 mmol) in dichloromethane (3 mL) was added 2,6-lutidine (78 μL, 0.67 mmol) and TBSOTf (85 μL, 0.37 mmol) at 0 °C, and the mixture was stirred for 50 min at room temperature. To the resulting mixture was added 2,6-lutidine (40 μL) and TBSOTf (50 μL) additionally at room temperature. The reaction mixture was diluted with H_2O, and extracted with ethyl acetate. The organic layer was washed with brine, and the extracts were dried over $MgSO_4$, filtered, and concentrated *in vacuo*. The residue was purified by silica gel chromatography (hexane–ethyl acetate = 50 : 1) to give **24** (62.4 mg, 0.13 mmol, 38%). $[\alpha]_D^{24}$ = −20.7 (*c* 0.8, $CHCl_3$); ^{1}H NMR (400 MHz, $CDCl_3$) δ 5.95–5.83 (m, 1H), 5.15–5.08 (m, 2H), 4.69 (d, *J* = 10.1 Hz, 1H), 4.29–4.22 (m, 1H), 3.97 (t, *J* = 8.7 Hz, 1H), 3.78 (t, *J* = 9.2 Hz, 1H), 2.47–2.25 (m, 2H), 2.01 (t, J = 2.7 Hz, 1H), 1.41 (s, 9H), 0.91 (s, 9H), 0.88 (s, 9H), 0.12 (d, *J* = 4.6 Hz, 6H), 0.05 (s, 6H); ^{13}C NMR (100 MHz, $CDCl_3$) δ 155.8, 139.4, 117.4, 80.6, 78.9, 76.0, 70.7, 69.2, 57.2, 28.4, 25.9, 25.2, 18.1, −2.9, −4.1, −4.5, −4.6; HRMS: calcd for $C_{25}H_{49}NO_4Si_2Na$, 506.3098; found, 506.3075.

Vinyl ketone 26. To a solution of **25** (5.80 g, 20.1 mmol) in THF (40 mL) was added vinylmagnesium bromide (1 M in THF, 25 mL, 25 mmol) at 0 °C, and the mixture was stirred for 2 h at room temperature. The resulting mixture was quenched by 1 N HCl at 0 °C and extracted with ethyl acetate. The organic layer was washed with brine, and the extracts were dried over $MgSO_4$, filtered, and concentrated *in vacuo*. The residue was purified by silica gel chromatography (hexane–ethyl acetate = 10 : 1) to give **26** (4.37 g, 17.1 mmol, 85%). $[\alpha]_D^{20}$ = −33.0 (*c* 0.7, $CHCl_3$); ^{1}H NMR (300 MHz, $CDCl_3$) δ 6.56 (ddd, *J* = 10.3, 17.2, 17.2 Hz, 1H), 6.34 (dd, *J* = 4.4, 17.2 Hz, 1H), 5.85 (dd, *J* = 1.3, 10.3 Hz, 1H), 4.78–4.53 (m, 1H), 4.23–4.13 (m, 1H), 4.00–3.98 (m, 1H), 1.72–1.34 (m, 15H); ^{13}C NMR (100 MHz, $CDCl_3$) δ 196.7 151.3 131.8 129.9 95.2 80.7 65.6 63.9 28.3 28.2; HRMS: (ESI, M + Na^+) calcd for $C_{13}H_{21}NO_4Na$, 278.1368; found, 278.1360.

TBS ether 27. To a solution of **26** (334.5 mg, 1.31 mmol) in diethyl ether (13 mL) was added a 0.18 M diethyl ether solution of $Zn(BH_4)_2$ (5 mL) at −20 °C, and the mixture was stirred for 1 h. To the resulting mixture was added 1 N HCl at 0 °C and the mixture was extracted with ethyl acetate. The extracts were washed with brine, and the organics were dried over $MgSO_4$, filtered, and concentrated *in vacuo* to give alcohol (328.7 mg). To a solution of the resulting alcohol (328.7 mg) in DMF (2 mL) was added imidazole (215 mg, 3.16 mmol), TBSCl (238 mg, 1.58 mmol) and DMAP (16 mg, 0.132 mmol) at room temperature, and the mixture was stirred for 5 h. To the reaction mixture was added saturated $NaHCO_3$, and the mixture was extracted with ethyl acetate. The organic layer was washed with brine, and the extracts were dried over $MgSO_4$, filtered, and concentrated *in vacuo*. The residue was purified by silica gel chromatography (hexane–ethyl acetate = 50 : 1) to give **27** (434.7 mg, 1.17 mmol, 89% from **26**). $[\alpha]_D^{21}$ = −34.9 (*c* 1.2, $CHCl_3$); ^{1}H NMR (300 MHz, $CDCl_3$) δ 5.84–5.67 (m, 1H), 5.28–5.04 (m, 2H), 4.59–4.21 (m, 1H), 4.03 (d, *J* = 5.1 Hz, 1H), 3.90–3.83 (m, 1H), 3.83–3.71 (m, 1H), 1.46 (s, 9H), 0.88 (s, 9H), 0.00 (s, 6H); ^{13}C NMR (125 MHz, $CDCl_3$) δ 152.7, 152.1, 139.2, 138.9, 116.2, 115.5, 94.2, 94.0, 79.9, 79.7, 74.3, 71.9, 64.3, 63.1, 61.6, 61.4, 28.4, 26.7, 25.9, 25.8, 25.2, 23.2, 18.0, −4.4, −4.6; HRMS: (ESI, M + Na^+) calcd for $C_{19}H_{37}NO_4SiNa$, 394.2389; found, 394.2387.

Epoxide 28. A solution of **27** (3.12 g, 8.4 mmol) in dichloromethane (40 mL) and methanol (40 mL) was treated with ozone at −78 °C with stirring for 40 min. Then $NaBH_4$ (1.9 g, 50.4 mmol) was added to the resulting mixture, which was warmed up slowly to room temperature over 12 h. To the reaction mixture was added 3 N HCl, and the organic layer was extracted with dichloromethane. The extracts were dried over $MgSO_4$, filtered, and concentrated *in vacuo* to give alcohol (3.2 g). To a solution of the alcohol (3.2 g) in dichloromethane (30 mL) was added triethylamine (1.8 mL, 12.6 mmol) and methanesulfonyl chloride (1.3 mL, 16.8 mmol) at room temperature, and the mixture was stirred for 1.5 h. The resulting mixture was diluted with H_2O and extracted with dichloromethane, and the extracts were dried over $MgSO_4$, filtered, and concentrated *in vacuo*. The residue was purified by silica gel chromatography (hexane–ethyl acetate = 10 : 1) to give mesylate (3.59 g, 7.91 mmol, 94% from **27**). To a solution of mesylate (175.3 mg, 0.386 mmol) in THF (5 mL) was added TBAF (505 mg, 1.93 mmol) at room temperature, and the mixture was stirred for 10 min. To the reaction mixture was added saturated NH_4Cl, and the organic layer was extracted with ethyl acetate. The extracts were washed with brine, dried over $MgSO_4$, filtered, and concentrated *in vacuo*. The residue was purified by silica gel chromatography (hexane–ethyl acetate = 20 : 1) to give **28** (75.8 mg,

0.311 mmol, 81%). $[\alpha]_D^{22}$ = +12.5 (*c* 1.1, $CHCl_3$); ^{1}H NMR (400 MHz, $CDCl_3$) δ 4.10–3.95 (m, 2H), 3.61–3.38 (m, 1H), 3.00 (s, 1H), 2.89 (s, 1H), 2.86–2.70 (m, 1H), 1.69–1.42 (m, 15H); ^{13}C NMR (100 MHz, $CDCl_3$) δ 152.3, 151.7, 94.3, 93.7, 80.4, 80.0, 66.0, 65.4, 59.2, 58.9, 52.3, 51.9, 48.3, 48.2, 28.3, 28.2, 27.4, 26.6, 24.2, 23.0; HRMS: (ESI, M + Na^+) calcd for $C_{12}H_{21}NO_4Na$, 266.1368; found, 266.1361.

Silyl ether 29. To a solution of trimethylsilylacetylene (1.6 mL, 11.3 mmol) in THF (45 mL) was added *n*-butyllithium (1.6 M in hexane, 6.8 mL, 11.3 mmol) at 0 °C, and the mixture was stirred for 10 min. To the reaction mixture was added a solution of **28** (1.83 g, 7.53 mmol) in THF (15 mL) and BF_3–Et_2O (1.9 mL, 15.0 mmol) at −78 °C. After being stirred for 1 h, triethylamine (10 mL, 75.2 mmol) was added to the resulting mixture. The reaction mixture was warmed to room temperature, and concentrated *in vacuo*. The residue was filtered through a pad of silica gel using ethyl acetate to give alcohol (2.32 g, 6.78 mmol, 90%). To a solution of alcohol (2.21 g, 6.47 mmol) in DMF (1 mL) was added imidazole (1.7 g, 25.9 mmol) and TBDPSCl (2.5 mL, 9.71 mmol) at room temperature, and the mixture was stirred at 40 °C for 8 h. To the reaction mixture was added saturated $NaHCO_3$, and the organic layer was extracted with ethyl acetate. The extracts were washed with brine, dried over $MgSO_4$, filtered, and concentrated *in vacuo*. The residue was purified by silica gel chromatography (hexane–ethyl acetate = 100 : 1) to give **29** (3.63 g, 6.26 mmol, 97%). $[\alpha]_D^{17}$ = −61.0 (*c* 1.7, $CHCl_3$); ^{1}H NMR (300 MHz, $CDCl_3$) δ 7.75–7.67 (m, 4H), 7.45–7.34 (m, 6H), 4.46 (dd, *J* = 8.3, 2.1 Hz, 1H), 4.33–4.20 (m, 1H), 4.04–3.91 (m, 2H), 2.23–2.12 (m, 2H), 1.59–1.35 (m, 15H), 1.08 (s, 9H), 0.12 (s, 9H); ^{13}C NMR (125 MHz, $CDCl_3$) δ 153.2, 152.4, 135.8, 135.7, 134.7, 134.2, 129.7, 129.6, 127.6, 127.5, 103.6, 103.1, 94.3, 93.6, 87.2, 79.9, 71.2, 70.7, 63.5, 62.3, 61.1, 28.4, 27.0, 26.4, 19.4, −0.06; HRMS: (ESI, M + Na^+) calcd for $C_{33}H_{49}NO_4Si_2Na$, 602.3097; found, 602.3079.

Allyl alcohol 30. To a solution of **29** (3.63 g, 6.26 mmol) in acetonitrile (40 mL) was bismuth tribromide (281 mg, 0.626 mmol) at room temperature, and the mixture was stirred for 1 h. To the reaction mixture was added H_2O (0.1 mL) at room temperature and the mixture was stirred for 30 min. To the resulting mixture was added saturated $NaHCO_3$, and the organic layer was extracted with ethyl acetate. The extracts were washed with brine, dried over $MgSO_4$, filtered, and concentrated *in vacuo*. The residue was purified by silica gel chromatography (hexane–ethyl acetate = 10 : 1) to give alcohol (3.09 g, 5.72 mmol, 91%). To a solution of the alcohol (322 mg, 0.596 mmol) in dichloromethane (6 mL) was added NMO (83 mg, 0.709 mmol) and MS 4Å (330 mg) at room temperature, then TPAP (23 mg, 0.0656 mmol) was added and the resulting mixture was stirred for 20 min. The reaction mixture was filtered through a pad of silica gel using ethyl acetate, and eluted fractions were concentrated *in vacuo* to give aldehyde (297.1 mg, 0.550 mmol, 92%). To a solution of the aldehyde (212.4 mg, 0.513 mmol) in THF (5 mL) was added vinylmagnesium bromide (1 M in THF, 1.5 mL, 1.5 mmol) at 0 °C, and the mixture was stirred for 30 min. To the reaction mixture was added 1 N HCl at 0 °C, and organic layer was extracted with ethyl acetate. The extracts were washed with brine, dried over $MgSO_4$, filtered, and concentrated *in vacuo*. The residue was purified by silica gel chromatography (hexane–ethyl acetate = 20 : 1) to give **30** (79.3 mg, 0.179 mmol, 35%). $[\alpha]_D^{25}$ = −12.8 (*c* 1.2, $CHCl_3$); ^{1}H NMR (300 MHz, $CDCl_3$) δ 7.70–768 (m, 4H), 7.49–7.38 (m, 6H), 5.78 (ddd, *J* = 16.6, 10.9, 5.4 Hz, 1H), 5.39–5.29 (m, 2H), 5.16 (d, *J* = 10.3 Hz, 1H), 4.81–4.78 (m, 1H), 4.12–4.09 (m, 1H), 3.76–3.74 (m, 1H), 2.41 (dd, *J* = 17.7 6.3 Hz, 1H), 2.34 (dd, *J* = 17.7, 4.6 Hz, 1H), 1.40 (s, 9H), 1.10 (s, 9H), 0.13 (s, 9H); ^{13}C NMR (125 MHz, $CDCl_3$) δ 155.9, 137.2, 135.8, 132.8, 132.1, 130.1, 127.8, 115.8, 102.3, 88.2, 79.2, 73.0, 70.9, 56.9, 28.3, 26.9, 25.5, 19.3, −0.12; HRMS: (ESI, M + Na^+) calcd for $C_{32}H_{47}NO_4Si_2Na$, 588.2941; found, 588.2934.

Amine 31. To a solution of **30** (665.4 mg, 1.18 mmol) in THF (10 mL) was added TBAF (771 mg, 2.95 mmol) at room temperature, and the mixture was stirred for 40 min. To the reaction mixture was added saturated NH_4Cl, and the mixture was extracted with ethyl acetate. The organic layer was washed with brine, and the extracts were dried over $MgSO_4$, filtered, and concentrated *in vacuo*. The residue was purified by silica gel chromatography (hexane–ethyl acetate = 2 : 1) to give diol (268.6 mg, 1.05 mmol, 89%). To the diol (268.6 mg, 1.05 mmol) was added a mixed solution of TFA and dichloromethane (1 : 4, 5 mL) at 0 °C, and the mixture was stirred for 2 h at room temperature. The reaction mixture was concentrated *in vacuo* to give diol (309.3 mg). To a solution of the diol (309.3 mg) in dichloromethane (3 mL) was added 2,6-lutidine (1.4 mL, 12.6 mmol) and TBSOTf (1.2 mL, 5.25 mmol) at 0 °C, and the mixture was stirred for 8 h at room temperature. To the reaction mixture was added saturated $NaHCO_3$, and extracted with ethyl acetate. The organic layer was washed with H_2O and brine, dried over $MgSO_4$, filtered, and concentrated *in vacuo*. The residue was purified by silica gel chromatography (hexane–ethyl acetate = 50 : 1) to give **31** (278.1 mg, 0.726 mmol, 69% from the diol). $[\alpha]_D^{19}$ = −1.9 (*c* 1.0, $CHCl_3$); ^{1}H NMR (300 MHz, $CDCl_3$) δ 5.87 (ddd, *J* = 17.4, 10.5, 7.3 Hz, 1H), 5.21 (d, *J* = 17.4 Hz, 1H), 5.16 (d, *J* = 10.5 Hz, 1H), 4.12 (dd, *J* = 5.9, 7.3 Hz, 1H), 3.82 (ddd, *J* = 4.4, 4.4, 6.7 Hz, 1H), 2.83 (dd, *J* = 4.58, 5.50 Hz, 1H), 2.53 (dd, *J* = 17.4, 6.87, 2.75 Hz, 1H), 2.44 (dd, *J* = 17.4, 4.58, 2.75 Hz, 1H), 1.93 (t, *J* = 2.75 Hz, 1H), 0.89 (s, 9H), 0.88 (s, 9H), 0.11 (s, 3H), 0.075 (s, 3H), 0.068 (s, 3H), 0.030 (s, 3H); ^{13}C NMR (100 MHz, $CDCl_3$) δ 139.3, 116.5, 82.4, 75.0, 71.8, 69.8, 61.0, 25.9, 25.8, 22.5, 18.1, 18.0, −3.5, −3.7, −4.6, −4.7; HRMS: (ESI, M + H^+) calcd for $C_{20}H_{42}NO_2Si_2$, 384.2754; found, 384.2745.

2β-*N*,*N*′-Dibenzylamine 32. To a solution of **31** (30.4 mg, 0.0792 mmol) in acetonitrile (1 mL) was added K_2CO_3 (66 mg, 0.475 mmol) and BnBr (38 μL, 0.317 mmol) at room temperature, and the mixture was stirred for 1 h at 80 °C. To the reaction mixture was added NaI (14 mg, 0.095 mmol) at room temperature, and the mixture was stirred at 80 °C for 21 h. To the reaction mixture was added saturated NH_4Cl at room temperature, and organic layer was extracted with ethyl acetate. The extracts were washed with brine, dried over $MgSO_4$, filtered, and concentrated *in vacuo*. The residue was purified by silica gel chromatography (hexane–ethyl acetate = 100 : 1) to give **32** (24 mg,